



HAL
open science

Electrochemical oxidation treatment of Direct Red 23 aqueous solutions: Influence of the operating conditions

Fatima Ezzahra Titchou, Hicham Zazou, Hanane Afanga, Jamila El Gaayda, Rachid Ait Akbour, Geoffroy Lesage, M. Rivallin, Marc Cretin, Mohamed Hamdani

► **To cite this version:**

Fatima Ezzahra Titchou, Hicham Zazou, Hanane Afanga, Jamila El Gaayda, Rachid Ait Akbour, et al.. Electrochemical oxidation treatment of Direct Red 23 aqueous solutions: Influence of the operating conditions. *Separation Science and Technology*, 2022, 57 (9), pp.1501-1520. 10.1080/01496395.2021.1982978 . hal-03647331

HAL Id: hal-03647331

<https://hal.umontpellier.fr/hal-03647331>

Submitted on 11 Oct 2023

HAL is a multi-disciplinary open access archive for the deposit and dissemination of scientific research documents, whether they are published or not. The documents may come from teaching and research institutions in France or abroad, or from public or private research centers.

L'archive ouverte pluridisciplinaire **HAL**, est destinée au dépôt et à la diffusion de documents scientifiques de niveau recherche, publiés ou non, émanant des établissements d'enseignement et de recherche français ou étrangers, des laboratoires publics ou privés.

Electrochemical oxidation treatment of Direct Red 23 aqueous solutions: Influence of the operating conditions

Fatima Ezzahra Titchou^{a,*}, Hicham Zazou^a, Hanane Afanga^a, Jamila El Gaayda^a, Rachid Ait Akbour^a, Geoffroy Lesage^b, Matthieu Rivallin^b, Marc Cretin^{b,*}, Mohamed Hamdani^{a,*}

^a Ibn Zohr University, Faculty of Sciences, Chemical department, BO 8106 –Dakhla district, Agadir, Morocco.

^b Institut Européen des Membranes, IEM, Univ Montpellier, CNRS, ENSCM, Montpellier, France

*Corresponding authors:

marc.cretin@umontpellier.fr (M. Cretin)

hamdani.mohamed@gmail.com (M. HAMDANI)

titchoufatimaezzahra@gmail.com (F.E. TITCHOU)

1 **Abstract**

2 A comparative study of the degradation of Direct Red 23 (DR23) dye aqueous solutions by
3 **electrooxidation** was investigated using different anodes: **carbon graphite (CG)**, dimensionally
4 stable anode (DSA), Magnéli phase Ti_4O_7 , and boron doped diamond (BDD). Stainless steel
5 (SS) and **CG** plates were tested as cathodes. The effect of operating parameters on the
6 degradation kinetic of the dye was studied. In this study, NaCl and Na_2SO_4 were selected as
7 supporting electrolytes; the former was found to be more suitable for the degradation of
8 DR23. The degradation of the dye follows a pseudo-first-order kinetic in both media. Higher
9 total organic carbon (TOC) efficiency was achieved by BDD/**CG** cells. Thus, the treatment
10 efficiency obtained using a current density of 5 mA cm^{-2} , and DR23 concentration of 60 mg
11 L^{-1} was about 86 % using both NaCl and Na_2SO_4 electrolyte, at 6 h electrolysis time. The
12 energy consumptions per **g** TOC removed were found to be 2.05 and 2.6 kWh **g** $^{-1}$ TOC in
13 NaCl and Na_2SO_4 electrolytes, respectively.

14 **Keywords:** **Electrooxidation**, Direct Red 23 dye, organic degradation, mineralization,
15 wastewater treatment.

16 **1. Introduction**

17 Nowadays, organic dye pollutants become a serious threat to the environment. Even in a small
18 quantity, they present a source of turbidity, eutrophication, non-aesthetic pollution; and their
19 discharge is particularly troublesome. Dyes present a higher biochemical stability due to their
20 high molecular weight and aromatic rings which are difficult to eliminate [1]. Azo dyes
21 constitute a real problem to the aqueous system and human health due to their side effects
22 such as carcinogenicity, skin irritation, allergy, acute toxicity, and mutagenicity [2,3]. Several
23 means were investigated to treat wastewaters containing recalcitrant pollutants; conventional
24 ones are usually ineffective. Although usual treatments such as precipitation,

25 biodegradation coupled to membrane separation, coagulation, flocculation, adsorption [4–7],
26 and electrocoagulation [8–12] were experienced for discoloration, they have common
27 drawbacks of generating sludge [8,13]. To overcome these problems, electrochemical
28 advanced oxidation processes (EAOPs) present a promising way to treat persistent pollutants
29 [2,14,15] due to the unique characteristics such as high efficiency, high mineralization, and
30 nonhazardous waste produced [3]. The interest related to EAOPs application for water
31 treatment is linked to their easy manipulation being ecofriendly methods. In terms of
32 sustainability, their installations can be supplied by renewable energies [16–18]. These
33 technologies are easily automatable, viable, decentralizable and finally adaptable according to
34 the nature of the effluents to be treated. The duration of the treatment can be optimized
35 according to the biorefractoriness of the effluent to finally end up with a biodegradable
36 solution after treatment [19]. The driving force is the in-situ generation of highly oxidant
37 agents mainly $\cdot\text{OH}$ radicals with a higher oxidation potential (versus standard hydrogen
38 electrode (SHE)) $E^\circ (\cdot\text{OH}/\text{H}_2\text{O}) = 2.80 \text{ V/ SHE}$ [20–22]. These reactive entities are able to
39 destroy unselectively organic and organometallic contaminants until their complete
40 mineralization into CO_2 , water, and inorganic ions [23,24]. They are considered the main
41 oxidizing species for the removal of organic pollutants in EAOPs, where hydroxyl radicals
42 can be generated in the bulk solution (homogeneous $\cdot\text{OH}$, denoted $\cdot\text{OH}$) and/or at the anode
43 surface (heterogeneous $\cdot\text{OH}$, marked $\text{M}(\cdot\text{OH})$, where M refers to anode material) [25,26].
44 Depending on the used anode and its potential window for water discharge, $\text{M}(\cdot\text{OH})$ may be
45 physisorbed in case of non-active anodes and chemisorbed in case of active anodes [24–26].

46 Electrochemical oxidation (electrooxidation) is an environmentally friendly method for the
47 treatment of water and wastewater, constitutes a direct way to produce $\text{M}(\cdot\text{OH})$ radicals
48 without using chemicals, where electrons are the only reagents [27]. $\cdot\text{OH}$ production generally
49 requires higher O_2 overpotential anodes (M) (Eq. (1)) [2]. Several electrodes have been used

50 for the **electrooxidation** such as PbO₂, doped SnO₂, IrO₂, DSA (dimensionally stable anodes)
51 that are mainly mixed metal oxide anodes, or Pt and BDD (boron doped diamond) [20]. SnO₂
52 and PbO₂ electrodes have a short life-time service and release toxic ions to the solution [1]. Pt
53 electrode is expensive which prevents it from being used for the scale-up. On the other hand,
54 BDD, a non-active anode, presents a wide potential window for water discharge; that provides
55 a promising condition for industrial-scale wastewater treatment. **This** anode is able to generate
56 weakly physisorbed hydroxyl radical [1]. Moreover, it can generate relatively weak oxidants
57 such as reactive oxygen species O₃ and H₂O₂, chlorine species, peroxodisulfate (S₂O₈²⁻),
58 peroxodiphosphate (P₂O₈⁴⁻), or peroxodicarbonate (C₂O₆²⁻) species [28–31]. This non-active
59 anode exhibits a good chemical and electrochemical stability and a long life time service [1].
60 DSA, an active anode, formed by a mixture of metal oxides, has the property of generating
61 hydroxyl radicals and a higher electrocatalytic activity for chlorine evolution reaction [32].
62 This property is due to the redox reaction of the transition metal elements which act as active
63 sites for chlorine atom adsorption [1]. Comparing BDD and DSA activity, unlike BDD, DSA
64 has low ability to electro-generate **M(•OH)**. **It** has a high stability, large production of Cl₂, and
65 chlorine-oxygen species, which are endowed with lower oxidant power than •OH, but with
66 interesting activity [33]. Therefore, direct oxidation of organics presents a sluggish kinetic
67 reaction on DSA surface and the secondary reaction is favored [1]. Recently, ceramic
68 electrodes based on sub-stoichiometric TiO₂, especially, Ti₄O₇ were reported to be an
69 alternative to BDD anodes. They are characterized by a high electrical conductivity and a
70 low-cost due to their preparation using TiO₂, the most abundant feedstock on the planet [34].
71 Moreover, concerning their electrochemical efficiency, they behave as non-active anodes,
72 yielding to a higher electrochemical mineralization efficiency compared to DSA [35,34].
73 Table 1 shows a brief summary of the recent application of **electrooxidation** in the treatment
74 of targeted organic pollutants.



75 **(Table 1)**

76 Considering the negative effect of dyes to the environment, this paper aimed to study the
77 degradation and mineralization of Direct Red 23 (DR23) as an azo naphthalene dye from its
78 aqueous solution. It is well known that azo dyes, containing a double bond N=N, are toxic and
79 their by-products are carcinogenic and mutagenic to the life being. According to this, previous
80 papers reported its elimination using photocatalytic degradation [41–45], UV-assisted AOPs
81 [46], persulfate oxidation [47], UV/H₂O₂ process using carbon nanotube particles [48,49],
82 adsorption process [50], enzymatic process [51], photo-electro Fenton [52,53], **electro Fenton**
83 **[54]**, ozonation and ultrasonolysis processes [55]. Nevertheless, the degradation and
84 mineralization of DR23 using **electrooxidation** remain unstudied. **Electrooxidation**, the most
85 popular and low cost technique, is considered as an effective technique to treat dyeing
86 solutions since it can degrade it by in-situ **M(\cdot OH)** generation and/or by mediating active
87 oxidants [56]. It does not need any chemical reagent addition such as Fe²⁺ unlike the electro-
88 Fenton process. **Electrooxidation** efficiency depends on the operating conditions such as
89 temperature, pH, electrolyte medium, and electrode materials **[33,56–58]**. Therefore, this
90 work aims to study the discoloration and mineralization of DR23 aqueous solution using
91 **electrooxidation** as the most widely used and powerful electrochemical process. To the best of
92 our knowledge, degradation/incineration of this dye is not yet performed. **This study**
93 **compared the efficiency of its removal using different powerful known anodes. BDD anode is**
94 **known by its higher potential for the removal of organic pollutants. However, it main**
95 **drawback is its higher cost. Therefore, this comparative study can be useful to highlight the**
96 **possible use of other powerful anodes in order to achieve similar efficiencies of those of BDD**
97 **anode.** The effect of different operating conditions was studied under galvanostatic mode
98 using different anode/cathode cells in chloride and sulfate media. **As the concentration of salts**

99 (electrolytes) differs from an industry to another, the chosen concentrations fall in the range
100 of the used amounts in textile industry, presenting the minimum of supporting electrolyte that
101 promotes the easy follow of discoloration kinetic and prevents side reactions and ohmic drop
102 [59,60]. The amount of salts 25 mM NaCl (conductivity = 2.5 mS cm⁻¹) and 12.5 mM Na₂SO₄
103 (conductivity = 2.3 mS cm⁻¹) were chosen to perform all the experiments in a constant 25 g-
104 equivalent of supporting electrolyte medium. Discoloration experiments of the dye solutions
105 were achieved in various operating conditions using different anode materials to compare
106 their efficiency for the removal of DR23. The range of tested parameters was chosen based on
107 some pretests and on different relevant literatures [23,61]. Mineralization efficiency, based on
108 total organic carbon (TOC) measurement, mineralization current efficiency (MCE%), and
109 energy consumption during the electrolysis were investigated.

110

111 2. Materials and methods

112 Direct Red 23 (DR23), the chosen pollutant to formulate the synthetic wastewater, is
113 generally used in viscose cellulose fiber dyeing for silk, wool, paper, and pulp dyeing. It is an
114 azo naphthalene dye (C₃₅H₂₅N₇Na₂O₁₀S₂, molar mass of 813.73 g mol⁻¹, color index C.I.
115 29160), of analytical grade, purchased from Sigma Aldrich and used without any further
116 purification. Required amount of DR23 was dissolved in ultrapure water to prepare the
117 desired concentrations. Sodium hydroxide, sulfuric acid, sodium chloride, and sodium sulfate,
118 were analytical grades from Prolabo and Fluka. All solutions were prepared with ultrapure
119 water obtained from a Millipore Milli-Q system with resistivity > 18 MΩ cm at 25 °C.

120 2.1. Description of the electrochemical process

121 The elimination of DR23 by electrooxidation, in a batch study, was carried out with 230 mL
122 of the dye solution in a 250 mL Pyrex beaker. The electrolysis was performed in an undivided

123 electrolytic cell where different electrode combinations were used. All used electrodes except
124 for Ti_4O_7 anode were purchased from different suppliers. Four anodes were tested:
125 dimensionally stable anode (DSA), ($\text{Ti}/\text{RuO}_2\text{-IrO}_2$ (4 cm \times 6 cm \times 0.2 cm) from Baoji Xinyu
126 Guang Ji Dian Limited Liability Company, China), which can be prepared as reported by Yu
127 et al. [62], boron doped diamond (BDD) thin-film deposited on a niobium substrate (4 cm \times 6
128 cm \times 0.2 cm) from CONDIAS, Germany, fabricated as described by Fryda et al. [63], carbon
129 graphite (CG)(expanded graphite sheet PSB-860, (4 cm \times 6 cm \times 0.4 cm), purchased from
130 SHIELD SEALING & Packing CO., LTD, China, prepared as indicated by Liu et al. [64],
131 and Ti_4O_7 (4 cm \times 6 cm \times 0.2 cm) thin film deposited on Ti substrate from Saint Gobain
132 Research Provence (France) prepared as described elsewhere [65,66]. Ti_4O_7 was synthesized
133 by plasma coating of prepared TiO_x ($x < 2$) particles (20–60 μm) on a Ti substrate (4 cm \times 6
134 cm) as described by Ganiyu et al. [65]. Ti substrate surface was pretreated by sandblasting in
135 order to obtain a rough surface. By applying coating conditions reported by Ganiyu et al. [65],
136 a continuous thick film of 100 μm and 95% density was achieved. The prepared electrode
137 mainly contains Ti_4O_7 phase with the presence of TiO_2 rutile and Ti_3O_5 as indicated by X-ray
138 diffraction. The plasma-sprayed coating has a typical electronic conductivity of 10^3 S cm^{-1} .
139 The tested cathodes were CG (4 cm \times 6 cm \times 0.4 cm), and AINSI 304 Stainless steel (SS)
140 plate (4 cm \times 6 cm \times 0.4 cm). Electrolysis was conducted under galvanostatic conditions, by
141 applying a constant current using a digital DC supply unit, ELC model ALR3002M. For all
142 electrodes, 30 cm^2 is kept constant as the submerged geometric surface area. The distance
143 between these electrodes was 1.5 cm, and they were connected to the DC power supply. The
144 pH variation was monitored using HANNA pH meter. Prior to each experiment, compressed
145 air (Flow air, 1.5 L min^{-1}) was bubbled for 10 min through the cell to saturate the solution
146 with dissolved oxygen. All electrolyses were performed in triplicate and averaged at room

147 temperature (20 ± 2 °C), and the solutions were homogenized with magnetic stirring (600 rpm)
148 during the treatment to allow efficient mass transfer.

149 2.2. Analytical procedure

150 The discoloration was monitored using Shimadzu spectrophotometer UV-VIS 1800 at the
151 maximum adsorption wavelength ($\lambda_{\max} = 502$ nm), to assess the decrease in chromophore
152 absorption bands by taking different aliquots of 2 mL at different times. Calibration curve of
153 DR23 absorbance was prepared using known aqueous solutions with different concentrations
154 (20, 30, 40, 60, 80, 100, and 200 mg L⁻¹). The color removal was computed using (Eq. (2)):

$$\text{Color removal (\%)} = \left(\frac{A_0 - A_t}{A_0} \right) \times 100 \quad (2)$$

155 where A_0 and A_t are the initial and final dye absorbance.

156 Total Organic Carbon (TOC) measurements were determined by injecting samples of 50 μ L
157 through thermal catalytic oxidation at 680 °C using TOC-L SHIMADZU analyzer equipped
158 with a manual injector. The TOC removal was then calculated using (Eq. (3)):

$$\text{TOC removal (\%)} = \frac{\text{TOC}_0 - \text{TOC}}{\text{TOC}_0} \times 100 \quad (3)$$

159 where TOC_0 and TOC stand for the initial and TOC (mg L⁻¹) at a given reaction time,
160 respectively.

161 The mineralization current efficiency, MCE%, was estimated by (Eq. (4)) [67]:

$$\text{MCE\%} = \frac{nFV_s\Delta(\text{TOC})_{\text{exp}}}{4.32 \times 10^7 \times m \times I \times t} \times 100 \quad (4)$$

162 where F is the Faraday constant (96487 C mol⁻¹), V_s is the solution volume (L), $\Delta(\text{TOC})_{\text{exp}}$ is
163 the experimental TOC change (mg L⁻¹) at a given time, 4.32×10^7 is an homogenization factor

164 (3600 s h⁻¹ × 12,000 mg of C mol⁻¹), m is the number of carbon atoms of DR23 (35 atoms), I is
165 the applied current (A) and t is the electrolysis time (h). n is the electron transfer number per
166 mole of DR23 taken as 138 considering the total mineralization according to the following
167 reaction Eq. (5):



168 The energy consumption, EC, (kWh g⁻¹ TOC) was determined using (Eq. (6)) [68]:

$$\text{EC (kWh g}^{-1}\text{ TOC)} = \frac{E_{\text{cell}} I t}{(\text{TOC}_0 - \text{TOC}_t) V_s} \quad (6)$$

169 where E_{cell} is the average voltage applied (V), I is the applied current intensity (A), t is the
170 treatment time (h), TOC₀ and TOC_t are the TOC values (mg L⁻¹) at the initial time and at a
171 given electrolysis time t, respectively, and V_s is the solution volume (L). In all trials,
172 degradation was monitored using UV-Vis technique while mineralization was followed by
173 TOC-meter.

174 3. Results and discussion

175 3.1. Parameters influencing the degradation of DR23

176 3.1.1. Effect of electrode materials and supporting electrolyte

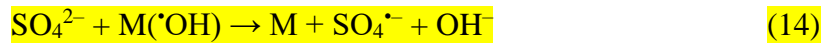
177 Although electrooxidation is a process essentially based on the power of the anode in the
178 electrolytic cell, the cathode can help improve the efficiency of the process, which depends on
179 the nature of the electrode used. The electrode materials influence the degradation rate of
180 organic pollutants since their efficiency depends on their ability to generate oxidizing species
181 such as M(•OH) and/or chlorine and sulfate active species on the anode and H₂O₂ on the
182 cathode. The former species are the main oxidizing agents for the destruction of pollutants.
183 Therefore, this study focused on the role of the nature of the anode and cathode materials in
184 addition to the supporting electrolyte to set the effective combination to get rid of DR23.

185 Therefore, four anodes including dimensionally stable anode (DSA), boron-doped diamond
186 (BDD), Ti_4O_7 , and CG, were tested and compared using CG, and stainless steel (SS) as
187 cathodes. The degradation was carried out using 40 mg L^{-1} DR23, 8.3 mA cm^{-2} current
188 density, and 25 mM NaCl or $12.5 \text{ mM Na}_2\text{SO}_4$, at natural pH ($\text{pH} = 6.0$), to set the effect of
189 electrode combination, Figure 1. In all cases, color removal increased progressively with
190 electrolysis time and this increase depends on the added salt. In these trials, the pH remained
191 almost constant with variations close to ± 0.3 pH units in Na_2SO_4 medium, whereas it changes
192 in NaCl where the final pH evolves to be near to neutral at the end of electrolysis, in the case
193 of BDD and DSA, and acidic for Ti_4O_7 . The drop of the pH to acidic values using Magnéli
194 Ti_4O_7 may have a beneficial effect on the stability of hydroxyl radicals that requires acidic
195 conditions [69]. Similar observation was already reported by Salazar et al. [33] indicating that
196 the active chlorine evolution changes the final pH of the solution as a function of electrodes
197 and electrolysis time.

198 Comparing the activity of anode materials, DSA, Ti_4O_7 , and BDD anodes show a higher
199 degradation activity compared to CG, whatever the medium. Although the CG anode may
200 contribute to the degradation of DR23 by the $\text{M}(\cdot\text{OH})$ radicals formed, during electrolysis, its
201 surface burns over time, damaging it and limiting its reuse. Carbon-based materials such as
202 CG undergo incineration, and their corrosion depends on various parameters such as pH,
203 current and the presence of NaCl . This corrosion occurs even at low currents [70,71].

204 Regarding the electrolytic media, the higher discoloration activity was found in NaCl
205 supporting electrolyte. In the presence of sulfate ions, compared to DSA anode, BDD and
206 Ti_4O_7 are known being able to generate reactive sulfate species, $\text{S}_2\text{O}_8^{2-}$ and $\text{SO}_4^{\cdot-}$, depending
207 on the pH and applied current density, through direct oxidation on the anode surface or the
208 reaction with $\text{M}(\cdot\text{OH})$ (Eqs. (7)-(15)(12)) [72–76]. The electro-generated sulfate active
209 species may contribute to the solution degradation in addition to the strong oxidant $\text{M}(\cdot\text{OH})$

210 radicals [72,77–79]. However, for DSA, the lower degradation efficiency could be attributed
211 to the strong adsorption of $M(\cdot\text{OH})$ that can limit the discoloration rate [33].

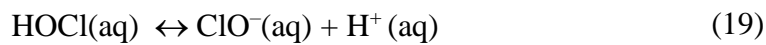
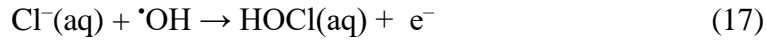


212 These sulfate active species are known by their higher standard potential being 2.01 V/SHE
213 for $\text{S}_2\text{O}_8^{2-}$ and 2.6 V/SHE for $\text{SO}_4^{\cdot-}$ [72,80,81]. However, the higher bleaching properties of
214 chloride active species compared to sulfate active species are reported in many cases. For
215 example, the effects of different electrolytes (NaCl , Na_2SO_4 , Na_2CO_3 , and HClO_4) on Alizarin
216 Red S (ARS) degradation using BDD anode, were studied and compared. A fast complete
217 discoloration of ARS was achieved within 6 min using NaCl electrolyte [82].

218 Regarding the obtained results, the NaCl supporting electrolyte was used for further
219 investigations on the degradation of DR23.

220 In the case of BDD and DSA anodes, the presence of NaCl leads to generate electro-active
221 chlorine oxidizing species such as Cl_2 , HClO , and ClO^- , once chloride ions undergo oxidation

222 as reported by Degaki et al. [83] and Jalife-Jacobo et al. [56] following the reactions (Eqs.
 223 (16)-(19)). Furthermore, the low evolution of chlorine on DSA surface favors the generation
 224 of active chlorine species during the oxidation of chlorides [68].



225 It should be noted that the stability of these oxidizing agents in the solution depends on its pH.
 226 The pK_a of HOCl/ClO⁻ couple is given equal to 7.55 [68]. Globally, chlorine, Cl₂ is the
 227 predominant species when pH < 3.00, hypochlorous acid, HOCl for 3.00 < pH < 7.50, and
 228 hypochlorite ion, ClO⁻ for pH > 7.55 [67,84]. However, other species of chlorine, ClO₂⁻,
 229 ClO₃⁻ and ClO₄⁻, with low oxidizing power were mentioned in the literature [85].
 230 However, in the case of Ti₄O₇, the oxidation of Cl⁻ according to Eq. (16) do not occurs on
 231 Ti₄O₇ surface as reported by Wang et al. [86]. They reported that the degradation of organics
 232 is mainly attributed to M([•]OH) radicals formed at the anode surface beside the synergic effect
 233 of chlorine active species formed as follow: (Eqs. (20)-(24)).



234 Moreover, in terms of reactivity, they reported that hydroxyl radicals are more reactive than
 235 the produced chlorine species. Their lower reactivity leads to their accumulation in the cell

236 with less oxidation potential to form ClO^- , ClO_2^- , ClO_3^- , and ClO_4^- as presented in Eqs. ((25)-
237 (28)) [87].



238 Regarding the negative impact of ClO_3^- and ClO_4^- on health (disturbance of the normal
239 functions of the thyroid gland and carcinogenic effect) [86], the low production of these
240 species in the case of Ti_4O_7 present an advantage for this electrode for their large scale
241 application in **electrooxidation** of organic pollutants [86].

242 As it can be seen in **Figure 1**, the highest degradation of DR23 is obtained using DSA/**CG**
243 system in the presence of chloride ions. In this case, the discoloration of the solution results
244 mainly from the dye's chromophore destruction by active chlorine species which are formed
245 at the testing pH solution. Similar results are carried out by others studying the degradation of
246 Reactive Blue 19 dye using a BDD or DSA anode in a flow reactor [83].

247 The oxidation power of DSA/**CG** and DSA/SS are almost similar, the difference is due to the
248 contribution of **CG** cathode which may generate H_2O_2 (Eq. (29)) unlike the SS cathode which
249 promotes mainly oxygen reduction via 4 transferred electrons. It is well known that cathodes
250 made of carbon materials promote the formation of H_2O_2 via two-electron oxygen reduction
251 reaction (ORR) at low current density according to the reaction (Eq. (29)) **[88,89]**. The
252 generation of oxidant species, H_2O_2 on the cathode is more favorable in acidic medium. In
253 addition, carbonaceous materials have significant catalytic performance for accelerating the
254 activation of in-situ generated H_2O_2 into hydroxyl radicals that enhances the degradation and
255 mineralization efficiency [90,91].



256 Sopaj et al. [92] stated that the stainless steel cathode generates very low H₂O₂ amounts, for
257 the operating conditions, current densities of 2.4 to 5 mA cm⁻², Pt anode, 50 mM Na₂SO₄, pH
258 = 3.00, under continuous air bubbling conditions. In the previous work, the hydrogen
259 peroxide amount was determined by titration of the complex (1:1) formed between Ti(IV) and
260 H₂O₂ by measuring its color intensity in acidic media, at a wavelength of 423 nm.

261 Likewise, the difference of discoloration efficiency obtained for both Ti₄O₇ and BDD using
262 CG and SS cathodes could be interpreted by the generation of H₂O₂ on CG surface. As
263 presented in the Figure 1, the discoloration in the case of Ti₄O₇ is almost coincident with that
264 of DSA. Similar result was observed by He et al. [93] using Ti₄O₇ and DSA anode for the
265 discoloration of methyl orange solution. In NaCl medium, the discoloration follows the order:
266 DSA/CG ≈ Ti₄O₇/CG > DSA/SS ≈ Ti₄O₇/SS > BDD/CG > BDD/SS. The lower degradation
267 in the case of Ti₄O₇ and BDD compared to DSA anode can be attributed to the consumption
268 of M(•OH) due to chlorine (Eqs. ((25)-(28)) [34]. In contrast, active anodes, endowed with
269 high oxygen evolution overpotential, the oxidation of target molecules mainly occurs directly
270 on the anode surface by the adsorbed hydroxyl radicals electro-generated according to
271 reaction (Eq. (1)). However, the oxidation rate strongly depends on the applied current density
272 and mass transfer in the cell as the pollutants must reach the anode surface [1]. It was reported
273 that the oxidation of pollutants by M(•OH) generated by inactive anodes leads to high removal
274 efficiency; these reacting species are adsorbed physically onto the anode surface and react
275 with the pollutant in the interface of solid/solution [94,95]. Hence, the treatment cost may
276 increase according to the electrolysis time. The use of effective intermediate oxidizing agents
277 obtained by electro-generating active chlorine species leads to indirect oxidation by mass
278 transfer to the bulk of the solution, which hinders the above limitation. Based on these
279 assertions, color removal is principally dependent on the active chlorine species

280 concentrations produced by the used electrodes as suggested by Salazar et al. [33]. These
281 authors recognized that the production of chlorine species on DSA anodes is higher than what
282 was generated on BDD anodes whatever the pH and current density. Similar results were
283 carried out by Malpass et al. [96] using BDD and DSA anodes for the degradation of both the
284 pesticide atrazine and cyanuric acid by **electrooxidation** in NaCl and Na₂SO₄ supporting
285 electrolytes. Therefore, DSA, Ti₄O₇, or BDD anode, and **CG** as the cathode were chosen to
286 study the operating conditions effect on the degradation of DR23 for the sake of comparison
287 in NaCl medium.

288

289 **(Figure 1)**

290

291 *3.1.2. Effect of NaCl concentration*

292 The study of NaCl electrolyte deserves special attention since Cl⁻ has an ubiquitous character
293 [15]. The electrical conductivity of the solution plays an important role in the degradation
294 reaction. Good conductivity leads to a faster electron transfer, a better degradation ratio, and
295 energy saving [8,69]. In chloride media, the reduction of organic compounds occurs mainly
296 by indirect oxidation other than direct oxidation, due to strong in-situ electro-generated
297 reactants, which may transform target pollutants into less harmful compounds. As was already
298 reported before, the main oxidizing agents are active chlorine, hypochlorous acid, or
299 hypochlorite ions, those reactants are produced anodically from chloride as indicated in
300 reactions (Eqs. ((16)-(19)) [1,8]. It is well known that increasing the concentration of the
301 supporting electrolyte affects color removal, which positively impacts the conductivity of the
302 solution and reduces the cell voltage leading to decrease the energy consumption.

303 To study the effect of supporting electrolyte on the removal of 60 mg L⁻¹ of DR23, different
304 concentrations of NaCl, 12.5, 25, 50, and 75 mM were investigated. Experiments were carried

305 out under 5 mA cm^{-2} current density and at natural pH of the solution ($\text{pH} = 6.0 \pm 0.4$), for
306 DSA/CG, $\text{Ti}_4\text{O}_7/\text{CG}$, and BDD/CG cells, as shown in Figure 2a, 2b, and 2c, respectively. The
307 same behavior was observed for DSA, Ti_4O_7 , and BDD, the color removal increases when the
308 concentration of NaCl increases, illustrating the positive impact on the degradation of DR23.
309 The enhancement of the efficiency is related to the increase of production-mediated oxidants
310 and the decrease of the selectivity for oxygen evolution due to the increase of Cl^-
311 concentration as reported by Jager et al. [39].

312 The total discoloration requires 40 min for a concentration of 12.5 mM of NaCl where it
313 requires only 20 min using 50 mM or 75 mM of NaCl in all electrolytic cells tested. On the
314 other hand, the discoloration rate is slower for BDD/CG system compared to DSA/CG and
315 $\text{Ti}_4\text{O}_7/\text{CG}$, in the same operating conditions. The kinetic of discoloration fits with the pseudo-
316 first order kinetic model with R^2 almost equal to unity. As shown in Figure 2d, the kinetic
317 rates enhance from 0.080 to 0.173 min^{-1} , from 0.079 to 0.197 min^{-1} , and from 0.069 to 0.1514
318 min^{-1} when the concentration of NaCl increases from 12.5 to 75 mM, for Ti_4O_7 , DSA and
319 BDD, respectively. The higher kinetic rate in the case of DSA anode and especially for 75
320 mM of NaCl is related to the higher accumulation of active chlorine species formed in the
321 medium. This behavior is in complete agreement with the reported literature of the
322 degradation of organic compounds being enhanced with NaCl concentration [97–100]. As
323 mentioned by Ganiyu et al. [73] the generation of reactive chlorine species is particularly high
324 using DSA anodes. However, in the case of BDD, less active chlorine species can be
325 simultaneously generated by the action of $\text{M}(\cdot\text{OH})$ according to the reactions (Eqs. ((25)-
326 (28)), where ClO_3^- and ClO_4^- are considered as unwanted by-products [85,101]. These species
327 were endowed with low oxidizing power, they limit the electrochemical degradation of
328 organics and constitute a scavenger for hydroxyl radicals as reported by Dominguez et al.
329 [85]. Furthermore, the higher kinetic rates in the case of Ti_4O_7 may be attributed to the less

330 formation of ClO_3^- and ClO_4^- and the stability of hydroxyl radicals under acidic conditions as
331 mentioned before.

332 **(Figure 2)**

333

334 *3.1.3. Effect of current density*

335 The current density is a direct controlled parameter; it affects the degradation rate and the
336 energy consumption. Figure 3a, 3b, and 3c present the current density variation effect on the
337 elimination rate of 60 mg L⁻¹ of DR23 using 25 mM of NaCl at pH = 6.0 for DSA, BDD, and
338 Ti₄O₇ anodes, respectively. The increase in the current density enhances the color removal
339 and regulates the ability of hydroxyl radical and active chlorine generation on anode surfaces
340 [56,102,103]. The total discoloration occurred around 40 min for a density of 2.5 mA cm⁻²
341 and decreased to be only 10 min using 15 mA cm⁻² on the tested anodes. However, the
342 discoloration is almost faster in the case of DSA/CG system; this is due to the greater electro-
343 generation of active chlorine species [1]. The apparent kinetic rates increased about three
344 times from 0.055 to 0.291 min⁻¹, from 0.045 to 0.237 min⁻¹, and from 0.0831 to 0.182 min⁻¹
345 when the current density increased from 2.5 to 15 mA cm⁻², for DSA/CG, BDD/CG, and
346 Ti₄O₇/CG cells, respectively, Figure 3d. Similarly, the electrochemical oxidation kinetic rate
347 of Acid Brown 98 using Ti/Ru_{0.3}Ti_{0.7}O₂ composite anode increases from 0.036 to 0.062 min⁻¹
348 when the current density increases from 5 to 20 mA cm⁻² [99]. Likewise, Paniza et al. [1]
349 investigated a comparison between indirect oxidation on DSA anode and direct oxidation on
350 BDD surface of Acid Brown 98, they reported that the degradation enhanced with increasing
351 the current density for both electrodes while the discoloration of the solution is almost faster
352 on DSA anode. Regarding K_{app} values, Ti₄O₇ anode leads to a faster degradation compared to
353 DSA and BDD anode in similar operating conditions under lower current densities (2.5 and 5
354 mA cm⁻²). However, applying a current density above 5 mA cm⁻² could not further increase

355 the discoloration of DR23 solutions in the case of Ti_4O_7 , where the apparent kinetic rates
356 exhibit little changes. For higher current densities (10 and 15 $mA\ cm^{-2}$) K_{app} follows the order:
357 $K_{app} (DSA) > K_{app} (BDD) > K_{app} (Ti_4O_7)$. This result was consistent with the degradation of
358 tetracycline using Ti/Ti_4O_7 anode [104]. This behavior can be attributed to the limited mass
359 transfer rate of DR23 toward the Ti_4O_7 at a higher current density and/or, to some extent,
360 enhances some side reactions such as O_2 evolution and increases the energy consumption
361 [104,105].

362 (Figure 3)

363

364 3.1.4. Effect of the concentration of DR23

365 Figure 4a, 4b, and 4c present the effect of the concentration of DR23 on the color removal,
366 using 25 mM NaCl and 5 $mA\ cm^{-2}$ as the current density. As the concentration of dyes in
367 textile wastewater is ranged from 5 to 230 $mg\ L^{-1}$ as reported by Yaseen et al. [60], the tested
368 concentrations of DR23 were 60, 80, 100, and 200 $mg\ L^{-1}$. The increase of the initial
369 concentration decreases either the efficiency of the discoloration, Figure 4a, 4b, and 4c, and
370 the kinetic rate Figure 4d. The apparent kinetic rate constants decreased from 0.101 to 0.070
371 min^{-1} , from 0.093 to 0.065 min^{-1} , and from 0.134 to 0.046 min^{-1} when the concentrations of
372 DR23 increased from 60 to 200 $mg\ L^{-1}$ in DSA/CG, BDD/CG, and Ti_4O_7/CG cells,
373 respectively. Generally, longer times of treatment are required to attain the same color
374 removal efficiency with the increase of the initial concentration of DR23, due to the
375 considerable slower discoloration rate at higher pollutant load [2]. This behavior can be
376 related to the greater amount of organics in solution to react with the similar amount of
377 oxidizing species, associated with the propensity of dye molecules to form clusters at high
378 concentration, thus decreasing dye diffusion rate to the anode surface [106]. With the increase
379 of DR23 concentration, the accumulation of intermediates and by-products is expectable,

380 which are thereafter competing with the colored compounds to react with the same amount of
381 active chlorine in the case of DSA and either with $M(OH)$ in the case of BDD and Ti_4O_7
382 anodes. Consequently, a smaller proportion of organics compared to the initial pollutant
383 concentration is oxidized. Abdel-Aziz et al. [106] reported that increasing the initial
384 concentration of dyes from 50 to 100 $mg L^{-1}$ decreased the color removal from 60 to 41% and
385 from 70 to 46% for methylene blue and methyl blue, respectively, during the first 10 min of
386 treatment using 2.5 $g L^{-1}$ of NaCl at $pH = 3$ and under 42.55 $mA cm^{-2}$. Similar behavior was
387 also reported elsewhere with increasing concentration of organic pollutants [98].

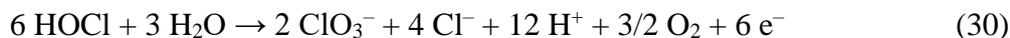
388 **(Figure 4)**

389

390 3.1.5. Effect of initial pH

391 Figure 5a, 5b, and 5c present the effect of initial pH on the color removal of 60 $mg L^{-1}$ of
392 DR23 using 25 mM NaCl under a current density of 5 $mA cm^{-2}$. The higher color removal
393 efficiency is achieved at $pH = 3.00$ using DSA/CG system. When the initial pH increased, the
394 effectiveness of the degradation decreases dramatically by increasing the pH from 5.00 to
395 11.00. For BDD/CG cell, the effectiveness of the degradation remains sensibly constant in the
396 pH range of 3.00 to 9.00, while it decreased slightly at $pH = 11.00$. Therefore, the direct
397 oxidation of DR23 on the BDD anode is efficient over a wide pH range. Serrano [107]
398 reported the effect of acidic pH on the performance of the discoloration of the solution and
399 explained the faster oxidation in the presence of active chlorine. This behavior is related to
400 oxidizing power given by the standard potential of each produced chloride species, i.e. HOCl
401 and Cl_2 have the highest standard potential ($E^\circ (HOCl/Cl^-) = 1.49 V/SHE$) compared to Cl_2
402 ($E^\circ (Cl_2/Cl^-) = 1.36 V/SHE$) and ClO^- ($E^\circ (ClO^-/Cl^-) = 0.89 V/SHE$). In addition, Rajkumar
403 et al. [98] attributed the decrease of the efficiency of the elimination of Reactive Blue 19 in
404 chloride medium using DSA anode to the decreased production of chlorine/hypochlorite at

405 higher pH conditions, due to the formation of chlorate or perchlorate with a low oxidizing
406 potential according to the following reactions (Eqs. (30), (31)).



407 The pH variation during electrolysis can be attributed to the formation of these species (insert
408 panels (Figure 5a and 5b)). In the case of the Magnéli phase Ti_4O_7 (Figure 5c), the
409 degradation of DR23 was highly influenced by the initial pH value. The best efficiency was
410 obtained for $\text{pH} = 3$ and it decreased with increasing the pH value. After 30 min of
411 electrolysis time the discoloration achieved was 97%, 97%, 95%, 94%, and 84% using pH 3,
412 5, 7, 9, and 11, respectively.

413 The pH drops during the first 30 min in the case of Ti_4O_7 contrarily to the case of using DSA
414 and BDD anodes (insert panel (Figure 5c)). This behavior can be attributed to the slow
415 formation of ClO_3^- and ClO_4^- on the surface of Ti_4O_7 due to the absence of **direct oxidation of**
416 Cl^- , where it is mainly oxidized according to Eq. (20) and (21) [86]. This fact was also
417 observed by Wang et al. in the case of perfluoroalkyl acids treatment using Ti_4O_7 , where they
418 reported that no appreciable chlorate and perchlorate was formed during the first 8 h of the
419 treatment [87]. Similar results was observed by Gui et al. [108] in the case of methyl orange
420 degradation.

421 Wang et al. [86] observed the higher accumulation of free chlorine using Ti_4O_7 compared to
422 BDD anode suggesting their less readily oxidation potential on the Ti_4O_7 , which highlights its
423 advantage in application for electrochemical oxidation treatment of organic pollutants in
424 chloride medium.

425 However, to ensure the maximum mineralization efficiency in the subsequent part, the
426 solution pH will be adjusted to acidic (pH = 3.00) during the electrolysis. In general, it is well
427 known that hydroxyl radical formation is better in acidic media [26,69]. Therefore, the higher
428 efficiency at various solution pH promotes the practical implementation of **electrooxidation**
429 process to treat wastewaters.

430 (Figure 5)

431

432 3.2. Mineralization

433 3.2.1. Effect of electrode system on the mineralization efficiency of DR23

434 To determine the best treatment to eliminate DR23 by **electrooxidation**, the mineralization
435 efficiency was investigated. **Figure 6** presents a comparison of the mineralization efficiency of
436 DR23 in terms of TOC removal, using different electrode systems. Operating conditions were
437 fixed at 60 mg L⁻¹ of DR23, pH = 3.00, 5 mA cm⁻² with 25 mM of NaCl (**Figure 6a**) or 12.5
438 mM of Na₂SO₄ (**Figure 6b**). The pH value was maintained at 3.0 ± 0.3 by adding acidic
439 solution during the electrolysis time, in the case of NaCl medium. As shown in **Figure 6a** and
440 **6b**, TOC removal increased steadily for about 1.5 h before slowing down with prolonged
441 electrolysis time. The highest rate of TOC removal was achieved using BDD/**CG** system,
442 around 86% using either NaCl or Na₂SO₄ electrolytes, after 6 h of electrolysis. Meanwhile,
443 BDD/SS system, whose activity comes just below the former, presents the mineralization
444 efficiency of 73 and 82 % in NaCl and Na₂SO₄ electrolytes, respectively, under similar
445 experimental conditions. It is evidenced that the use of **CG** cathode enhanced the breakdown
446 of DR23 in NaCl medium, with a relative increase of 18%, unlike Na₂SO₄, which may be
447 attributed to the activity of **CG** cathode to generate H₂O₂, contributing to the mineralization of
448 the dye. Furthermore, for all other systems, the use of **CG** cathodes allows higher TOC

449 removals than those of SS cathodes, in the same operating conditions. DSA/CG cell, endowed
450 with a good activity in degradation, presents the worst mineralization efficiencies in chlorine
451 and sulfate medium; they reached only 25 and 28 % TOC removal respectively. Between the
452 two extreme results, Ti₄O₇/CG, Ti₄O₇/SS, CG/SS and CG/CG systems present intermediate
453 efficiencies. However, Ti₄O₇/CG and Ti₄O₇/SS yield to a close efficiency to that of BDD
454 anode in NaCl medium. After 6h of electrolysis time, TOC removals achieved using
455 Ti₄O₇/CG and Ti₄O₇/SS were 60 and 51% in NaCl and 44 and 42% in Na₂SO₄, respectively.
456 CG/SS and CG/CG reached 36 and 39 % in NaCl electrolyte and reached 45 and 51 % in
457 Na₂SO₄ electrolyte, respectively. Several authors have suggested that the mineralization
458 process is improved using a chloride ion as a supporting electrolyte [20,56]. Oturan [25]
459 reported that BDD thin film anode has a higher oxidation and/or mineralization power for the
460 treatment of organic pollutants in sulfate medium. This is due to the generation of physisorbed
461 M(OH) which are more available for destruction of organics than in the case of metallic
462 oxide anodes and DSA. Active anodes such as DSA and graphite have a low value of oxygen
463 evolution overpotential and permit only the partial oxidation of organics [109]. Salazar et al.
464 [33] compared the mineralization of Disperse Yellow 3 dye on BDD, Ti/Ru_{0.3}Ti_{0.7}O₂, and
465 Ti/Pt anodes in Na₂SO₄ and NaCl supporting electrolytes and achieved 90% TOC removal
466 with BDD in sulfate solution, while the percentage is up to 50% for other anodes, irrespective
467 of the operating conditions. They reported that DSA anode is more active in NaCl medium,
468 followed by BDD and Ti/Pt due to higher production of effective chlorine species which
469 depend on pH and anode material. Likewise, Yang et al. [110] reported that the order of the
470 mineralization of Imatinib drug decreases in the order: BDD > Ti₄O₇ > Pt > DSA. They
471 evaluated the TOC removal efficiency in Na₂SO₄ media, achieving total mineralization at 8 h
472 treatment using BDD anode. They also mentioned that the mineralization rate was 61%, 78%,
473 and 82% by Pt, DSA, and Ti₄O₇ anodes, respectively.

474 DR23 mineralization in BDD/CG system is mainly occurred by direct and mediated
475 electrochemical oxidation on the BDD surface in sulfate and in chloride media, respectively.
476 Physisorbed $M(\bullet OH)$ radicals, the strong oxidant, are considered as the main oxidant in
477 sulfate solution, while homogenous oxidation prevails in the chloride solution in the bulk of
478 the solution or near the anode surface. The trend of the TOC removal curve obtained by
479 BDD/CG in NaCl medium, Figure 6a, unlike in Na_2SO_4 , Figure 6b, shows that the
480 mineralization can still increase with the electrolysis time, confirming that the by-products are
481 still breakdown. Jalife-Jacobo et al. [56] have found the same results studying the degradation
482 of diazo dye congo red on BDD/SS cell and reported a favorable synergy between the free
483 $M(\bullet OH)$ and the active chlorine species leading to a faster mineralization using NaCl. On the
484 other hand, various by-products may be formed which are highly recalcitrant to oxidation by
485 the action of $M(\bullet OH)$ generated conjugated to that of oxidant species such as persulfates in
486 Na_2SO_4 medium.

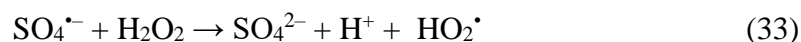
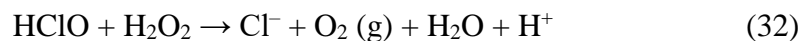
487 Based on (Eq. (6)), the energy consumption per g of TOC removed is presented in Figure 6c
488 using different electrode cells at 5 mA cm^{-2} after 6h electrolysis time. The energy
489 consumption, EC, at the end of electrolysis using BDD/CG is lower compared to other
490 systems. It is about 2.05 and 2.60 kWh g^{-1} TOC for NaCl and Na_2SO_4 , respectively. The same
491 trends which corroborate our findings were already reported [33]. This result highlights
492 clearly the low EC and the efficiency of BDD anode for DR23 treatment in solutions
493 containing chloride salts.

494 (Figure 6)

495

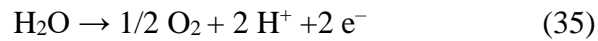
496 3.2.2. *Effect of current on the mineralization efficiency*

497 The effect of current density on TOC removal in the case of BDD/CG is presented in Figure
 498 7a and 7b for NaCl and Na₂SO₄, respectively. In the case of NaCl (Figure 7a), increasing the
 499 current density from 2.5 to 15 mA cm⁻² increases the TOC removal value and reduce the time
 500 required for total mineralization. After 6h, the obtained TOC removal values were 80%, 86%,
 501 94%, and 95% using 2.5, 5, 10, and 15 mA cm⁻², respectively. On the other hand, in the case
 502 of Na₂SO₄, the variation of TOC removal (%) vs. current density is shown in Figure 7b. As
 503 can be seen from the results, the increase of current density over 5 mA cm⁻² does not
 504 significantly improve the TOC removal % after 6h of electrolysis. The mineralization reached
 505 was 74%, 86%, 91%, and 92% using 2.5, 5, 10, and 15 mA cm⁻², respectively. The
 506 uncompleted mineralization can be attributed to the formation of recalcitrant and toxic by-
 507 products like chloroderivatives that are slowly degraded by active chlorine species and
 508 M(•OH), in the case of NaCl. In addition, the TOC removal efficiency can be affected by the
 509 consumption of M(•OH) by sulfate (Eqs. (13)-(15)) or chloride ions (Eq. (20)), and the
 510 decomposition of H₂O₂ by HOCl or SO₄^{•-} (formed through the reaction between sulfate ions
 511 and •OH (Eqs. (14), (15)) as presented in Eqs. (32)-(34) [111].



512 Besides the increase of the kinetic of TOC removal with the current density, the
 513 mineralization current efficiency, MCE%, decreased by increasing applied current density
 514 values, Figure 7c and 7d. MCE% values were significant for 2.5 mA cm⁻² at 2h of
 515 electrolysis; they were about 7.5% and 5.2% for NaCl and Na₂SO₄, respectively. For both
 516 electrolytes, increasing the electrolysis time reduces the MCE% due to the formation of short
 517 chain carboxylic acids that resist to the mineralization [61]. The increase in the current density

518 enhances the side reaction of oxygen evolution on BDD surface (Eq. (35)) as well as the
519 recombination of $\cdot\text{OH}$ in the bulk (Eq. (36)) or oxidation of $\text{M}(\cdot\text{OH})$ at the anode (Eq. (37))
520 [21].



521 To evaluate the feasibility of the process and the reliability of the electrodes, the energy
522 consumption, EC ($\text{kWh g}^{-1} \text{TOC}$) was computed using (Eq. 4) and its trend is presented in
523 [Figure 7e](#) and [7f](#). The increase of current density increases the energy consumption with
524 electrolysis time. It is clear from [Figure 7e](#) and [7f](#) that 5 mA cm^{-2} requires a low EC, about
525 $2.05 \text{ kWh g}^{-1} \text{TOC}$ and $2.6 \text{ kWh g}^{-1} \text{TOC}$ using NaCl and Na_2SO_4 , respectively, to achieve 86
526 % of TOC removal after 6h of electrolysis. From MCE% and the energy consumption, 5 mA
527 cm^{-2} was suggested as the optimal value for efficient mineralization of DR23 under fixed
528 experimental conditions.

529 **(Figure 7)**

530

531 **4. Conclusion**

532 In summary, the treatment of DR23 was investigated by **electrooxidation** process in a batch
533 reactor using different electrode configurations in operating conditions of current densities
534 ($2.5, 5, 10, \text{ and } 15 \text{ mA cm}^{-2}$) under values of pH about 3.00, 5.00, 6.00, 7.00, 9.00, and 11.00,
535 and 25 mM NaCl or 12.5 mM Na_2SO_4 as the supporting electrolyte, at $20 \text{ }^\circ\text{C}$. The
536 effectiveness of different electrode combinations was compared during the degradation and
537 mineralization of DR23 solution. The results demonstrate that using BDD, Ti_4O_7 , or DSA

538 anodes coupled with CG or SS cathode is found to be helpful for a good discoloration in NaCl
539 medium. In addition, the discoloration rate increases by increasing the electrolysis time,
540 current density, concentration of supporting electrolyte, and decreases by increasing the pH
541 and the concentration of the dye. The best mineralization efficiency obtained for DR23
542 solutions was achieved with the BDD/CG, followed by BDD/SS with slight efficiency when
543 using CG cathode in both saline solutions. The mineralization of 60 mg L⁻¹ of DR23 with
544 BDD/CG system reaches about 86% of TOC removal in either chloride or sulfate solution,
545 using 5 mA cm⁻² at 6 h of electrolysis time. From MCE% and the energy consumption, 5 mA
546 cm⁻² was suggested as an optimal value for efficient mineralization of DR23 under fixed
547 experimental conditions using BDD/CG system. The energy consumption and MCE% were
548 2.05 kWh g⁻¹ TOC and 2.5%, and 2.6 kWh g⁻¹ TOC and 2.6%, using NaCl and Na₂SO₄,
549 respectively, after 6h of treatment.

550 The future trend and perspective of this study should focus on the identification of aliphatic
551 intermediates and inorganic ions to propose a mineralization pathway of DR23 and
552 investigate the ecotoxicity assessment of the final effluent to verify that toxicity has been
553 efficiently removed. Likewise, electrochemical behavior of the studied anodes and formed
554 active species in chloride and sulfate salts seem to be of importance. In addition, a comparison
555 between electrooxidation and other processes such as electro-Fenton process will be
556 performed to enhance the efficiency and reduce the treatment time.

557

558 **Acknowledgements**

559 The authors would like to thank the University of Ibn Zohr Agadir for making all the
560 necessary resources available for this work. F.E. Titchou thanks CNRST for providing the
561 fellowship. This work is done in the framework of the European ERANET MED Water-
562 13_043 project SETPROper: (Sustainable treatment processes of effluents for reuse of water

563 in agriculture) with the financial support of MOROCCAN MESRSFC. The authors also thank
564 Saint Gobain CREE Company for supplying the Ti₄O₇ anodes.

565

566 **Conflict of interest**

567 On behalf of all authors, the corresponding author states that there is no conflict of interest.

568 **References**

- 569 [1] M. Panizza, A. Barbucci, R. Ricotti, G. Cerisola, Electrochemical degradation of
570 methylene blue, Sep. Purif. Technol. 54 (2007) 382–387.
571 <https://doi.org/10.1016/j.seppur.2006.10.010>.
- 572 [2] E. do Vale-Júnior, S. Dosta, I.G. Cano, J.M. Guilemany, S. Garcia-Segura, C.A.
573 Martínez-Huitle, Acid blue 29 decolorization and mineralization by anodic oxidation
574 with a cold gas spray synthesized Sn–Cu–Sb alloy anode, Chemosphere. 148 (2016) 47–
575 54. <https://doi.org/10.1016/j.chemosphere.2016.01.015>.
- 576 [3] Z. Yousefi, A. Zafarzadeh, R.A. Mohammadpour, E. Zarei, N. Mengelizadeh, A.
577 Ghezeli, Electrochemical removal of acid red 18 dye from synthetic wastewater using a
578 three-dimensional electrochemical reactor, Desalination Water Treat. 165 (2019) 352–
579 361. <https://doi.org/10.5004/dwt.2019.24502>.
- 580 [4] S. Chatterjee, N. Guha, S. Krishnan, A.K. Singh, P. Mathur, D.K. Rai, Selective and
581 Recyclable Congo Red Dye Adsorption by Spherical Fe₃O₄ Nanoparticles
582 Functionalized with 1,2,4,5-Benzenetetracarboxylic Acid, Sci. Rep. 10 (2020) 111.
583 <https://doi.org/10.1038/s41598-019-57017-2>.
- 584 [5] F.E. Titchou, R. Ait Akbour, A. Assabbane, M. Hamdani, Removal of cationic dye from
585 aqueous solution using Moroccan pozzolana as adsorbent: Isotherms, kinetic studies, and

- 586 application on real textile wastewater treatment, *Groundw. Sustain. Dev.* 11 (2020)
587 100405. <https://doi.org/10.1016/j.gsd.2020.100405>.
- 588 [6] R. Ait Akbour, J.E. Gaayda, F.E. Titchou, A. Khenifi, H. Afanga, A. Farahi, P.-S. Yap,
589 M.B.S. Forte, M. Hamdani, Adsorption of anionic dyes from aqueous solution using
590 polyelectrolyte PDAD-MAC- modified-montmorillonite clay, *Desalination Water Treat.*
591 208 (2020) 407–422. <https://doi.org/doi:10.5004/dwt.2020.26446>.
- 592 [7] J. El Gaayda, R. Ait Akbour, F.E. Titchou, H. Afanga, H. Zazou, C. Swanson, M.
593 Hamdani, Uptake of an anionic dye from aqueous solution by aluminum oxide particles:
594 Equilibrium, kinetic, and thermodynamic studies, *Groundw. Sustain. Dev.* 12 (2020)
595 100540. <https://doi.org/10.1016/j.gsd.2020.100540>.
- 596 [8] F.E. Titchou, H. Afanga, H. Zazou, R. Ait Akbour, M. Hamdani, Batch elimination of
597 cationic dye from aqueous solution by electrocoagulation process, *Mediterr. J. Chem.* 10
598 (2020) 1–12. <https://doi.org/10.13171/mjc10102001201163mh>.
- 599 [9] H. Afanga, H. Zazou, F.E. Titchou, Y. Rakhila, R. Ait Akbour, A. Elmchaouri, J.
600 Ghanbaja, M. Hamdani, Integrated electrochemical processes for textile industry
601 wastewater treatment: system performances and sludge settling characteristics, *Sustain.*
602 *Environ. Res.* 30 (2020) 2. <https://doi.org/10.1186/s42834-019-0043-2>.
- 603 [10] M.M. Emamjomeh, H.A. Jamali, Z. Naghdali, M. Mousazadeh, Efficiency of
604 Electrocoagulation, Sedimentation and Filtration Hybrid Process in Removing Chemical
605 Oxygen Demand and Turbidity from Carwash Industrial Wastewater: Optimization by
606 Response Surface Methodology, *J. Mazandaran Univ. Med. Sci.* 29 (2019) 106–120.
- 607 [11] M.M. Emamjomeh, H. Jamali, Z. Naghdali, M. Mousazadeh, Carwash wastewater
608 treatment by the application of an environmentally friendly hybrid system: an
609 experimental design approach, 160 (2019) 171–177.
610 <https://doi.org/10.5004/DWT.2019.24382>.

- 611 [12] M. Emamjomeh, S. Kakavand, H. Jamali, S.M. Alizadeh, M. Safdari, S.E.S. Mousavi,
612 K.S. Hashim, M. Mousazadeh, The treatment of printing and packaging wastewater by
613 electrocoagulation– flotation: the simultaneous efficacy of critical parameters and
614 economics, *Desalination Water Treat.* 205 (2020) 161–174.
615 <https://doi.org/10.5004/dwt.2020.26339>.
- 616 [13] F.E. Titchou, H. Zazou, H. Afanga, J. El Gaayda, R.A. Akbour, M. Hamdani, Removal
617 of Persistent Organic Pollutants (POPs) from Water and Wastewater by Adsorption and
618 Electrocoagulation Process, *Groundw. Sustain. Dev.* 13 (2021) 100575.
619 <https://doi.org/10.1016/j.gsd.2021.100575>.
- 620 [14] E. Petrucci, L. Di Palma, R. Lavecchia, A. Zuurro, Treatment of diazo dye Reactive
621 Green 19 by anodic oxidation on a boron-doped diamond electrode, *J. Ind. Eng. Chem.*
622 26 (2015) 116–121. <https://doi.org/10.1016/j.jiec.2014.11.022>.
- 623 [15] C.A. Martínez-Huitle, S. Ferro, Electrochemical oxidation of organic pollutants for the
624 wastewater treatment: direct and indirect processes, *Chem Soc Rev.* 35 (2006) 1324–
625 1340. <https://doi.org/10.1039/B517632H>.
- 626 [16] C.A. Martínez-Huitle, M. Panizza, Electrochemical oxidation of organic pollutants for
627 wastewater treatment, *Curr. Opin. Electrochem.* 11 (2018) 62–71.
628 <https://doi.org/10.1016/j.coelec.2018.07.010>.
- 629 [17] S.O. Ganiyu, C.A. Martínez-Huitle, The use of renewable energies driving
630 electrochemical technologies for environmental applications, *Curr. Opin. Electrochem.*
631 22 (2020) 211–220. <https://doi.org/10.1016/j.coelec.2020.07.007>.
- 632 [18] C. Candia-Onfray, S. Rojas, M.V.B. Zanoni, R. Salazar, An updated review of metal–
633 organic framework materials in photo(electro)catalytic applications: From CO₂
634 reduction to wastewater treatments, *Curr. Opin. Electrochem.* 26 (2021) 100669.
635 <https://doi.org/10.1016/j.coelec.2020.100669>.

- 636 [19] S.O. Ganiyu, C.A. Martínez-Huitle, M.A. Rodrigo, Renewable energies driven
637 electrochemical wastewater/soil decontamination technologies: A critical review of
638 fundamental concepts and applications, *Appl. Catal. B Environ.* 270 (2020) 118857.
639 <https://doi.org/10.1016/j.apcatb.2020.118857>.
- 640 [20] A. Thiam, I. Sirés, J.A. Garrido, R.M. Rodríguez, E. Brillas, Effect of anions on
641 electrochemical degradation of azo dye Carmoisine (Acid Red 14) using a BDD anode
642 and air-diffusion cathode, *Sep. Purif. Technol.* 140 (2015) 43–52.
643 <https://doi.org/10.1016/j.seppur.2014.11.012>.
- 644 [21] H. Zazou, N. Oturan, M. Sönmez Çelebi, M. Hamdani, M.A. Oturan, Cold incineration
645 of 1,2-dichlorobenzene in aqueous solution by electrochemical advanced oxidation using
646 DSA/Carbon felt, Pt/Carbon felt and BDD/Carbon felt cells, *Sep. Purif. Technol.* 208
647 (2019) 184–193. <https://doi.org/10.1016/j.seppur.2018.03.030>.
- 648 [22] I. Sirés, E. Brillas, Upgrading and expanding the electro-Fenton and related processes,
649 *Curr. Opin. Electrochem.* 27 (2021) 100686.
650 <https://doi.org/10.1016/j.coelec.2020.100686>.
- 651 [23] H. Afanga, H. Zazou, F.E. Titchou, J.E. Gaayda, F. Sopaj, R.A. Akbour, M. Hamdani,
652 Electrochemical oxidation of Naphthol Blue Black with different supporting electrolytes
653 using a BDD /carbon felt cell, *J. Environ. Chem. Eng.* 9 (2021) 104498.
654 <https://doi.org/10.1016/j.jece.2020.104498>.
- 655 [24] F.E. Titchou, H. Zazou, H. Afanga, J.E. Gaayda, R. Ait Akbour, P.V. Nidheesh, M.
656 Hamdani, An overview on the elimination of organic contaminants from aqueous
657 systems using electrochemical advanced oxidation processes, *J. Water Process Eng.* 41
658 (2021) 102040. <https://doi.org/10.1016/j.jwpe.2021.102040>.

- 659 [25] M.A. Oturan, Outstanding performances of the BDD film anode in electro-Fenton
660 process: Applications and comparative performance, *Curr. Opin. Solid State Mater. Sci.*
661 25 (2021) 100925. <https://doi.org/10.1016/j.cossms.2021.100925>.
- 662 [26] P.V. Nidheesh, M. Zhou, M.A. Oturan, An overview on the removal of synthetic dyes
663 from water by electrochemical advanced oxidation processes, *Chemosphere*. 197 (2018)
664 210–227. <https://doi.org/10.1016/j.chemosphere.2017.12.195>.
- 665 [27] C.A. Martínez-Huitle, M.A. Rodrigo, I. Sirés, O. Scialdone, Single and coupled
666 electrochemical processes and reactors for the abatement of organic water pollutants: A
667 critical review, *Chem. Rev.* 115 (2015) 13362–13407.
668 <https://doi.org/10.1021/acs.chemrev.5b00361>.
- 669 [28] Y. Yavuz, A. Savaş Koparal, Ü.B. Öğütveren, Electrochemical oxidation of Basic Blue 3
670 dye using a diamond anode: evaluation of colour, COD and toxicity removal, *J. Chem.*
671 *Technol. Biotechnol.* 86 (2011) 261–265. <https://doi.org/10.1002/jctb.2512>.
- 672 [29] J.L. Nava, F. Núñez, I. González, Electrochemical incineration of p-cresol and o-cresol
673 in the filter-press-type FM01-LC electrochemical cell using BDD electrodes in sulfate
674 media at pH 0, *Electrochimica Acta*. 52 (2007) 3229–3235.
675 <https://doi.org/10.1016/j.electacta.2006.09.072>.
- 676 [30] M. Villanueva-Rodríguez, A. Hernández-Ramírez, J.M. Peralta-Hernández, E.R.
677 Bandala, M.A. Quiroz-Alfaro, Enhancing the electrochemical oxidation of acid-yellow
678 36 azo dye using boron-doped diamond electrodes by addition of ferrous ion, *J. Hazard.*
679 *Mater.* 167 (2009) 1226–1230. <https://doi.org/10.1016/j.jhazmat.2008.12.137>.
- 680 [31] A.M.S. Solano, S. Garcia-Segura, C.A. Martínez-Huitle, E. Brillas, Degradation of
681 acidic aqueous solutions of the diazo dye Congo Red by photo-assisted electrochemical
682 processes based on Fenton's reaction chemistry, *Appl. Catal. B Environ.* 168–169 (2015)
683 559–571. <https://doi.org/10.1016/j.apcatb.2015.01.019>.

- 684 [32] S. Trasatti, Electrocatalysis: understanding the success of DSA®, *Electrochimica Acta*.
685 45 (2000) 2377–2385. [https://doi.org/10.1016/S0013-4686\(00\)00338-8](https://doi.org/10.1016/S0013-4686(00)00338-8).
- 686 [33] R. Salazar, M.S. Ureta-Zañartu, C. González-Vargas, C. do N. Brito, C.A. Martinez-
687 Huitle, Electrochemical degradation of industrial textile dye disperse yellow 3: Role of
688 electrocatalytic material and experimental conditions on the catalytic production of
689 oxidants and oxidation pathway, *Chemosphere*. 198 (2018) 21–29.
690 <https://doi.org/10.1016/j.chemosphere.2017.12.092>.
- 691 [34] S.O. Ganiyu, N. Oturan, S. Raffy, M. Cretin, C. Causserand, M.A. Oturan, Efficiency of
692 plasma elaborated sub-stoichiometric titanium oxide (Ti₄O₇) ceramic electrode for
693 advanced electrochemical degradation of paracetamol in different electrolyte media, *Sep.*
694 *Purif. Technol.* 208 (2019) 142–152. <https://doi.org/10.1016/j.seppur.2018.03.076>.
- 695 [35] S.O. Ganiyu, N. Oturan, S. Raffy, G. Esposito, E.D. van Hullebusch, M. Cretin, M.A.
696 Oturan, Use of Sub-stoichiometric Titanium Oxide as a Ceramic Electrode in Anodic
697 Oxidation and Electro-Fenton Degradation of the Beta-blocker Propranolol: Degradation
698 Kinetics and Mineralization Pathway, *Electrochimica Acta*. 242 (2017) 344–354.
699 <https://doi.org/10.1016/j.electacta.2017.05.047>.
- 700 [36] A. El-Ghenymy, F. Centellas, J.A. Garrido, R.M. Rodríguez, I. Sirés, P.L. Cabot, E.
701 Brillas, Decolorization and mineralization of Orange G azo dye solutions by anodic
702 oxidation with a boron-doped diamond anode in divided and undivided tank reactors,
703 *Electrochimica Acta*. 130 (2014) 568–576.
704 <https://doi.org/10.1016/j.electacta.2014.03.066>.
- 705 [37] S. Ammar, R. Abdelhedi, C. Flox, C. Arias, E. Brillas, Electrochemical degradation of
706 the dye indigo carmine at boron-doped diamond anode for wastewaters remediation,
707 *Environ. Chem. Lett.* 4 (2006) 229–233. <https://doi.org/10.1007/s10311-006-0053-2>.

- 708 [38] M. Hamza, R. Abdelhedi, E. Brillas, I. Sirés, Comparative electrochemical degradation
709 of the triphenylmethane dye Methyl Violet with boron-doped diamond and Pt anodes, J.
710 Electroanal. Chem. 627 (2009) 41–50. <https://doi.org/10.1016/j.jelechem.2008.12.017>.
- 711 [39] D. Jager, D. Kupka, M. Vaclavikova, L. Ivanicova, G. Gallios, Degradation of Reactive
712 Black 5 by electrochemical oxidation, Chemosphere. 190 (2018) 405–416.
713 <https://doi.org/10.1016/j.chemosphere.2017.09.126>.
- 714 [40] G. Wang, Y. Liu, J. Ye, Z. Lin, X. Yang, Electrochemical oxidation of methyl orange by
715 a Magnéli phase Ti₄O₇ anode, Chemosphere. 241 (2020) 125084.
716 <https://doi.org/10.1016/j.chemosphere.2019.125084>.
- 717 [41] S. Song, L. Xu, Z. He, H. Ying, J. Chen, X. Xiao, B. Yan, Photocatalytic degradation of
718 C.I. Direct Red 23 in aqueous solutions under UV irradiation using SrTiO₃/CeO₂
719 composite as the catalyst, J. Hazard. Mater. 152 (2008) 1301–1308.
720 <https://doi.org/10.1016/j.jhazmat.2007.08.004>.
- 721 [42] R. Byberg, J. Cobb, L.D. Martin, R.W. Thompson, T.A. Camesano, O. Zahraa, M.N.
722 Pons, Comparison of photocatalytic degradation of dyes in relation to their structure,
723 Environ. Sci. Pollut. Res. 20 (2013) 3570–3581. [https://doi.org/10.1007/s11356-013-](https://doi.org/10.1007/s11356-013-1551-y)
724 [1551-y](https://doi.org/10.1007/s11356-013-1551-y).
- 725 [43] D.N. Clausen, I.S. Scarmínio, K. Takashima, Optimization and effects of some electron
726 acceptors on the photocatalytic degradation of direct red 23 azo dye, J. Chil. Chem. Soc.
727 54 (2009) 289–294. <https://doi.org/10.4067/S0717-97072009000300018>.
- 728 [44] L. Ghalamchi, M.H. Rasoulifard, Immobilization of Fe₃O₄/TiO₂ nanocomposite thin
729 layer on the glass tubes in a component parabolic collector for the treatment of DR23,
730 Int. J. Environ. Sci. Technol. 16 (2019) 7509–7522. [https://doi.org/10.1007/s13762-018-](https://doi.org/10.1007/s13762-018-2169-x)
731 [2169-x](https://doi.org/10.1007/s13762-018-2169-x).

- 732 [45] N. Sobana, K. Selvam, M. Swaminathan, Optimization of photocatalytic degradation
733 conditions of Direct Red 23 using nano-Ag doped TiO₂, *Sep. Purif. Technol.* 62 (2008)
734 648–653. <https://doi.org/10.1016/j.seppur.2008.03.002>.
- 735 [46] I. Grčić, S. Papić, D. Mesec, N. Koprivanac, D. Vujević, The kinetics and efficiency of
736 UV assisted advanced oxidation of various types of commercial organic dyes in water, *J.*
737 *Photochem. Photobiol. Chem.* 273 (2014) 49–58.
738 <https://doi.org/10.1016/j.jphotochem.2013.09.009>.
- 739 [47] N. Liu, L. Zhang, Y. Xue, J. Lv, Q. Yu, X. Yuan, Nitrogen-doped carbon material as a
740 catalyst for the degradation of direct red23 based on persulfate oxidation, *Sep. Purif.*
741 *Technol.* 184 (2017) 213–219. <https://doi.org/10.1016/j.seppur.2017.04.045>.
- 742 [48] M. Torkaman, R. Moradi, B. Keyvani, Photocatalytic degradation azo dye direct red 23
743 using carbon nanotubes particles by uv/h₂o₂ process in batch photoreactor, *Rev. Roum.*
744 *Chim.* 61 (2016) 763-772.
- 745 [49] N.M. Mahmoodi, Photocatalytic Degradation of Dyes Using Carbon Nanotube and
746 Titania Nanoparticle, *Water. Air. Soil Pollut.* 224 (2013) 1612.
747 <https://doi.org/10.1007/s11270-013-1612-3>.
- 748 [50] B. Hayati, N.M. Mahmoodi, M. Arami, F. Mazaheri, Dye Removal from Colored Textile
749 Wastewater by Poly(propylene imine) Dendrimer: Operational Parameters and Isotherm
750 Studies: Dye Removal from Colored Textile Wastewater, *CLEAN - Soil Air Water.* 39
751 (2011) 673–679. <https://doi.org/10.1002/clen.201000182>.
- 752 [51] N. Khan, Q. Husain, Continuous degradation of Direct Red 23 by calcium pectate–
753 bound *Ziziphus mauritiana* peroxidase: identification of metabolites and degradation
754 routes, *Environ. Sci. Pollut. Res.* 26 (2019) 3517–3529. [https://doi.org/10.1007/s11356-](https://doi.org/10.1007/s11356-018-3847-4)
755 [018-3847-4](https://doi.org/10.1007/s11356-018-3847-4).

- 756 [52] A.R. Khataee, B. Vahid, B. Behjati, M. Safarpour, Treatment of a dye solution using
757 photoelectro-fenton process on the cathode containing carbon nanotubes under
758 recirculation mode: Investigation of operational parameters and artificial neural network
759 modeling, *Environ. Prog. Sustain. Energy.* 32 (2013) 557–563.
760 <https://doi.org/10.1002/ep.11657>.
- 761 [53] Reza Moradi, Amin Ganjali, Synthesis of Fe₃O₄ Nanoparticles and Their Application in
762 Photo-Fenton Degradation of Direct Red 23 Dye in Aqueous Solutions, *Russ. J. Phys.*
763 *Chem. A.* 93 (2019) 2789–2797. <https://doi.org/10.1134/S0036024419130211>.
- 764 [54] F.E. Titchou, H. Zazou, H. Afanga, J.E. Gaayda, R. Ait Akbour, M. Hamdani, M.A.
765 Oturan, Electro-Fenton process for the removal of Direct Red 23 using BDD anode in
766 chloride and sulfate media, *J. Electroanal. Chem.* (2021) 115560.
767 <https://doi.org/10.1016/j.jelechem.2021.115560>.
- 768 [55] M. Mohajerani, M. Mehrvar, F. Ein-Mozaffari, Correlation and prediction of azo dye
769 degradation by nonlinear least-square regression in combined ozonation and
770 ultrasonolysis processes, *Water Qual. Res. J.* 46 (2011) 250–258.
771 <https://doi.org/10.2166/wqrjc.2011.128>.
- 772 [56] H. Jalife-Jacobo, R. Feria-Reyes, O. Serrano-Torres, S. Gutiérrez-Granados, J.M.
773 Peralta-Hernández, Diazo dye Congo Red degradation using a Boron-doped diamond
774 anode: An experimental study on the effect of supporting electrolytes, *J. Hazard. Mater.*
775 319 (2016) 78–83. <https://doi.org/10.1016/j.jhazmat.2016.02.056>.
- 776 [57] S. Liu, H. Song, S. Wei, Q. Liu, X. Li, X. Qian, Effect of direct electrical stimulation on
777 decolorization and degradation of azo dye reactive brilliant red X-3B in biofilm-
778 electrode reactors, *Biochem. Eng. J.* 93 (2015) 294–302.
779 <https://doi.org/10.1016/j.bej.2014.11.002>.

- 780 [58] Z. Hu, J. Cai, G. Song, Y. Tian, M. Zhou, Anodic oxidation of organic pollutants: Anode
781 fabrication, process hybrid and environmental applications, *Curr. Opin. Electrochem.* 26
782 (2021) 100659. <https://doi.org/10.1016/j.coelec.2020.100659>.
- 783 [59] I. Bisschops, H. Spanjers, Literature review on textile wastewater characterisation,
784 *Environ. Technol.* 24 (2003) 1399–1411. <https://doi.org/10.1080/09593330309385684>.
- 785 [60] D.A. Yaseen, M. Scholz, Textile dye wastewater characteristics and constituents of
786 synthetic effluents: a critical review, *Int. J. Environ. Sci. Technol.* 16 (2019) 1193–1226.
787 <https://doi.org/10.1007/s13762-018-2130-z>.
- 788 [61] H. Zazou, N. Oturan, M. Sönmez Çelebi, M. Hamdani, M.A. Oturan, Cold incineration
789 of 1,2-dichlorobenzene in aqueous solution by electrochemical advanced oxidation using
790 DSA/Carbon felt, Pt/Carbon felt and BDD/Carbon felt cells, *Sep. Purif. Technol.* 208
791 (2019) 184–193. <https://doi.org/10.1016/j.seppur.2018.03.030>.
- 792 [62] N. Yu, X. Lu, F. Song, Y. Yao, E. Han, Electrocatalytic degradation of sulfamethazine
793 on IrO₂-RuO₂ composite electrodes: influencing factors, kinetics and modeling, *J.*
794 *Environ. Chem. Eng.* 9 (2021) 105301. <https://doi.org/10.1016/j.jece.2021.105301>.
- 795 [63] M. Fryda, Th. Mathee, S. Mulachy, M. Hofer, L. Schafer, I. Troster, Applications of
796 DIACHEM[®] Electrodes in Electrolytic Water Treatment, *Electrochem. Soc. Interface.*
797 12 (2003) 40–44. <https://doi.org/10.1149/2.F10031IF>.
- 798 [64] C. Liu, Z. Chen, H. Chen, Z. Miao, M. Fu, Preparation of expanded graphite-based
799 composites by one step impregnation, *J. Wuhan Univ. Technol.-Mater Sci Ed.* 26 (2011)
800 253–256. <https://doi.org/10.1007/s11595-011-0208-2>.
- 801 [65] S.O. Ganiyu, N. Oturan, S. Raffy, M. Cretin, R. Esmilaire, E. van Hullebusch, G.
802 Esposito, M.A. Oturan, Sub-stoichiometric titanium oxide (Ti₄O₇) as a suitable ceramic
803 anode for electrooxidation of organic pollutants: A case study of kinetics, mineralization

804 and toxicity assessment of amoxicillin, *Water Res.* 106 (2016) 171–182.
805 <https://doi.org/10.1016/j.watres.2016.09.056>.

806 [66] Y. Ouarda, C. Trelu, G. Lesage, M. Rivallin, P. Drogui, M. Cretin, Electro-oxidation of
807 secondary effluents from various wastewater plants for the removal of acetaminophen
808 and dissolved organic matter, *Sci. Total Environ.* 738 (2020) 140352.
809 <https://doi.org/10.1016/j.scitotenv.2020.140352>.

810 [67] E. Brillas, C.A. Martínez-Huitle, Decontamination of wastewaters containing synthetic
811 organic dyes by electrochemical methods. An updated review, *Appl. Catal. B Environ.*
812 166–167 (2015) 603–643. <https://doi.org/10.1016/j.apcatb.2014.11.016>.

813 [68] P. Saxena, J. Ruparelia, Influence of supporting electrolytes on electrochemical
814 treatability of reactive black 5 using dimensionally stable anode, *J. Inst. Eng. India Ser.*
815 *A.* 100 (2019) 299–310. <https://doi.org/10.1007/s40030-019-00360-4>.

816 [69] D. Li, J. Tang, X. Zhou, J. Li, X. Sun, J. Shen, L. Wang, W. Han, Electrochemical
817 degradation of pyridine by Ti/SnO₂–Sb tubular porous electrode, *Chemosphere.* 149
818 (2016) 49–56. <https://doi.org/10.1016/j.chemosphere.2016.01.078>.

819 [70] A.S. Abdalrhman, Electro-oxidation by graphite anode for naphthenic acids degradation,
820 biodegradability enhancement and toxicity reduction, *Sci. Total Environ.* 671 (2019)
821 270–279. <https://doi.org/10.1016/j.scitotenv.2019.03.262>

822 [71] M. Rueffer, D. Bejan, N.J. Bunce, Graphite: An active or an inactive anode?,
823 *Electrochimica Acta.* 56 (2011) 2246–2253.
824 <https://doi.org/10.1016/j.electacta.2010.11.071>.

825 [72] G. Divyapriya, P.V. Nidheesh, Electrochemically generated sulfate radicals by boron
826 doped diamond and its environmental applications, *Curr. Opin. Solid State Mater. Sci.*
827 25 (2021) 100921. <https://doi.org/10.1016/j.cossms.2021.100921>.

- 828 [73] S.O. Ganiyu, C.A. Martínez-Huitle, M.A. Oturan, Electrochemical advanced oxidation
829 processes for wastewater treatment: Advances in formation and detection of reactive
830 species and mechanisms, *Curr. Opin. Electrochem.* 27 (2021) 100678.
831 <https://doi.org/10.1016/j.coelec.2020.100678>.
- 832 [74] K.C. de Freitas Araújo, D.R. da Silva, E.V. dos Santos, H. Varela, C.A. Martínez-Huitle,
833 Investigation of persulfate production on BDD anode by understanding the impact of
834 water concentration, *J. Electroanal. Chem.* 860 (2020) 113927.
835 <https://doi.org/10.1016/j.jelechem.2020.113927>.
- 836 [75] D. Zhi, Y. Lin, L. Jiang, Y. Zhou, A. Huang, J. Yang, L. Luo, Remediation of persistent
837 organic pollutants in aqueous systems by electrochemical activation of persulfates: A
838 review, *J. Environ. Manage.* 260 (2020) 110125.
839 <https://doi.org/10.1016/j.jenvman.2020.110125>.
- 840 [76] J. Cai, T. Niu, P. Shi, G. Zhao, Boron-Doped Diamond for Hydroxyl Radical and Sulfate
841 Radical Anion Electrogenation, Transformation, and Voltage-Free Sustainable
842 Oxidation, *Small.* 15 (2019) 1900153. <https://doi.org/10.1002/sml.201900153>.
- 843 [77] S. Waclawek, H.V. Lutze, K. Grübel, V.V.T. Padil, M. Černík, Dionysios.D. Dionysiou,
844 Chemistry of persulfates in water and wastewater treatment: A review, *Chem. Eng. J.*
845 330 (2017) 44–62. <https://doi.org/10.1016/j.cej.2017.07.132>.
- 846 [78] J. Lee, U. von Gunten, J.-H. Kim, Persulfate-Based Advanced Oxidation: Critical
847 Assessment of Opportunities and Roadblocks, *Environ. Sci. Technol.* 54 (2020) 3064–
848 3081. <https://doi.org/10.1021/acs.est.9b07082>.
- 849 [79] G. Farshid, M. Mahsa, Application of peroxymonosulfate and its activation methods for
850 degradation of environmental organic pollutants: review, *Chem Eng J.* 310 (2017) 41–
851 62. <https://doi.org/10.1016/j.cej.2016.10.064>.

- 852 [80] K. Groenen Serrano, A critical review on the electrochemical production and use of
853 peroxy-compounds, *Curr. Opin. Electrochem.* 27 (2021) 100679.
854 <https://doi.org/10.1016/j.coelec.2020.100679>.
- 855 [81] S. Giannakis, K.-Y.A. Lin, F. Ghanbari, A review of the recent advances on the
856 treatment of industrial wastewaters by Sulfate Radical-based Advanced Oxidation
857 Processes (SR-AOPs), *Chem. Eng. J.* 406 (2021) 127083.
858 <https://doi.org/10.1016/j.cej.2020.127083>.
- 859 [82] C. Zhu, C. Jiang, S. Chen, R. Mei, X. Wang, J. Cao, L. Ma, B. Zhou, Q. Wei, G.
860 Ouyang, Z. Yu, K. Zhou, Ultrasound enhanced electrochemical oxidation of alizarin red
861 S on boron doped diamond (BDD) anode: Effect of degradation process parameters,
862 *Chemosphere.* 209 (2018) 685–695. <https://doi.org/10.1016/j.chemosphere.2018.06.137>.
- 863 [83] A.H. Degaki, G.F. Pereira, R.C. Rocha-Filho, N. Bocchi, S.R. Biaggio, Effect of
864 Specific Active Chlorine Species and Temperature on the Electrochemical Degradation
865 of the Reactive Blue 19 Dye Using a Boron-Doped Diamond or DSA Anode in a Flow
866 Reactor, *Electrocatalysis.* 5 (2014) 8–15. <https://doi.org/10.1007/s12678-013-0156-z>.
- 867 [84] C.Y. Cheng, G.H. Kelsall, Models of hypochlorite production in electrochemical
868 reactors with plate and porous anodes, *J. Appl. Electrochem.* 37 (2007) 1203–1217.
869 <https://doi.org/10.1007/s10800-007-9364-7>.
- 870 [85] C.M. Dominguez, N. Oturan, A. Romero, A. Santos, M.A. Oturan, Lindane degradation
871 by electrooxidation process: Effect of electrode materials on oxidation and
872 mineralization kinetics, *Water Res.* 135 (2018) 220–230.
873 <https://doi.org/10.1016/j.watres.2018.02.037>.
- 874 [86] L. Wang, J. Lu, L. Li, Y. Wang, Q. Huang, Effects of chloride on electrochemical
875 degradation of perfluorooctanesulfonate by Magnéli phase Ti₄O₇ and boron doped

876 diamond anodes, *Water Res.* 170 (2020) 115254.
877 <https://doi.org/10.1016/j.watres.2019.115254>.

878 [87] L. Wang, M. Nickelsen, S.-Y. (Dora) Chiang, S. Woodard, Y. Wang, S. Liang, R. Mora,
879 R. Fontanez, H. Anderson, Q. Huang, Treatment of perfluoroalkyl acids in concentrated
880 wastes from regeneration of spent ion exchange resin by electrochemical oxidation using
881 Magnéli phase Ti₄O₇ anode, *Chem. Eng. J. Adv.* 5 (2021) 100078.
882 <https://doi.org/10.1016/j.cej.2020.100078>.

883 [88] I. Diouf, O. Dia, M.B. Diedhiou, P. Drogui, A.O. Toure, S.M. Lo, M. Rumeau, C.G.
884 Mar/Diop, Electro-generation of hydrogen peroxide using a graphite cathode from
885 exhausted batteries: study of influential parameters on electro-Fenton process, *Environ.*
886 *Technol.* 41 (2020) 1434–1445. <https://doi.org/10.1080/09593330.2018.1537309>.

887 [89] O. García-Rodríguez, J.A. Bañuelos, A. Rico-Zavala, L.A. Godínez, F.J. Rodríguez-
888 Valadez, Electrocatalytic activity of three carbon materials for the In-situ production of
889 hydrogen peroxide and Its application to the electro-Fenton heterogeneous process, *Int.*
890 *J. Chem. React. Eng.* 14 (2016) 843–850. <https://doi.org/10.1515/ijcre-2015-0115>.

891 [90] W. Yang, M. Zhou, N. Oturan, Y. Li, P. Su, M.A. Oturan, Enhanced activation of
892 hydrogen peroxide using nitrogen doped graphene for effective removal of herbicide
893 2,4-D from water by iron-free electrochemical advanced oxidation, *Electrochimica Acta.*
894 297 (2019) 582–592. <https://doi.org/10.1016/j.electacta.2018.11.196>.

895 [91] E. Saputra, S. Muhammad, H. Sun, S. Wang, Activated carbons as green and effective
896 catalysts for generation of reactive radicals in degradation of aqueous phenol, *RSC Adv.*
897 3 (2013) 21905. <https://doi.org/10.1039/c3ra42455c>.

898 [92] F. Sopaj, N. Oturan, J. Pinson, F.I. Podvorica, M.A. Oturan, Effect of cathode material
899 on electro-Fenton process efficiency for electrocatalytic mineralization of the antibiotic

900 sulfamethazine, *Chem. Eng. J.* 384 (2020) 123249.
901 <https://doi.org/10.1016/j.cej.2019.123249>.

902 [93] W. He, Y. Liu, J. Ye, G. Wang, Electrochemical degradation of azo dye methyl orange
903 by anodic oxidation on Ti₄O₇ electrodes, *J. Mater. Sci. Mater. Electron.* 29 (2018)
904 14065–14072. <https://doi.org/10.1007/s10854-018-9538-6>.

905 [94] A. Kapalka, G. Fóti, C. Comninellis, The importance of electrode material in
906 environmental electrochemistry, *Electrochimica Acta.* 54 (2009) 2018–2023.
907 <https://doi.org/10.1016/j.electacta.2008.06.045>.

908 [95] M. Mascia, A. Vacca, S. Palmas, A.M. Polcaro, Kinetics of the electrochemical
909 oxidation of organic compounds at BDD anodes: modelling of surface reactions, *J. Appl.*
910 *Electrochem.* 37 (2006) 71–76. <https://doi.org/10.1007/s10800-006-9217-9>.

911 [96] G.R.P. Malpass, G.R. Salazar-Banda, D.W. Miwa, S.A.S. Machado, A.J. Motheo,
912 Comparing atrazine and cyanuric acid electro-oxidation on mixed oxide and boron-
913 doped diamond electrodes, *Environ. Technol.* 34 (2013) 1043–1051.
914 <https://doi.org/10.1080/09593330.2012.733420>.

915 [97] L. Gomes, D.W. Miwa, G.R.P. Malpass, A.J. Motheo, Electrochemical degradation of
916 the dye reactive orange 16 using electrochemical flow-cell, *J. Braz. Chem. Soc.* 22
917 (2011) 1299–1306. <https://doi.org/10.1590/S0103-50532011000700015>.

918 [98] D. Rajkumar, B.J. Song, J.G. Kim, Electrochemical degradation of Reactive Blue 19 in
919 chloride medium for the treatment of textile dyeing wastewater with identification of
920 intermediate compounds, *Dyes Pigments.* 72 (2007) 1–7.
921 <https://doi.org/10.1016/j.dyepig.2005.07.015>.

922 [99] S. Zeb, S. Hussain, H.A. Khan, Z. Ali, N. Khan, K.I. Khan, F. Ali, S. Khan, M. del P.T.
923 Sotomayo, S. Gul, Electrochemical Oxidation of Acid Brown 98 using Ti/Ru_{0.3}Ti_{0.7}O₂

- 924 Composite Anode, *Int. J. Electrochem. Sci.* 13 (2018) 9428–9440.
925 <https://doi.org/10.20964/2018.10.06>.
- 926 [100] D.F. Viana, G.R. Salazar-Banda, M.S. Leite, Electrochemical degradation of Reactive
927 Black 5 with surface response and artificial neural networks optimization models, *Sep.*
928 *Sci. Technol.* 53 (2018) 2647–2661. <https://doi.org/10.1080/01496395.2018.1463264>.
- 929 [101] C. do N. Brito, D.R. da Silva, S. Garcia-Segura, D.C. de Moura, C.A. Martínez-Huitle,
930 Indirect Electrochemical Oxidation of Reactive Blue 19 Dye as a Model Organic
931 Substrate: Role of Anode Material and Oxidants Electrochemically Generated, *J.*
932 *Electrochem. Soc.* 163 (2016) E62–E69. <https://doi.org/10.1149/2.0191603jes>.
- 933 [102] M.F. Murrieta, I. Sirés, E. Brillas, J.L. Nava, Mineralization of Acid Red 1 azo dye by
934 solar photoelectro-Fenton-like process using electrogenerated HClO and
935 photoregenerated Fe(II), *Chemosphere.* 246 (2020) 125697.
936 <https://doi.org/10.1016/j.chemosphere.2019.125697>.
- 937 [103] M. Panizza, M.A. Oturan, Degradation of Alizarin Red by electro-Fenton process
938 using a graphite-felt cathode, *Electrochimica Acta.* 56 (2011) 7084–7087.
939 <https://doi.org/10.1016/j.electacta.2011.05.105>.
- 940 [104] J. Wang, D. Zhi, H. Zhou, X. He, D. Zhang, Evaluating tetracycline degradation
941 pathway and intermediate toxicity during the electrochemical oxidation over a Ti/Ti4O7
942 anode, *Water Res.* 137 (2018) 324–334. <https://doi.org/10.1016/j.watres.2018.03.030>.
- 943 [105] J. Cai, M. Zhou, Y. Pan, X. Lu, Degradation of 2,4-dichlorophenoxyacetic acid by
944 anodic oxidation and electro-Fenton using BDD anode: Influencing factors and
945 mechanism, *Sep. Purif. Technol.* 230 (2020) 115867.
946 <https://doi.org/10.1016/j.seppur.2019.115867>.

947 [106] M.H. Abdel-Aziz, M. Bassyouni, M.S. Zoromba, A.A. Alshehri, Removal of dyes
948 from waste solutions by anodic oxidation on an array of horizontal graphite rods anodes,
949 *Ind. Eng. Chem. Res.* 58 (2019) 1004–1018. <https://doi.org/10.1021/acs.iecr.8b05291>.

950 [107] K. Groenen Serrano, Chapter 6 - Indirect Electrochemical Oxidation Using Hydroxyl
951 Radical, Active Chlorine, and Peroxodisulfate, in: C.A. Martínez-Huitle, M.A. Rodrigo,
952 O. Scialdone (Eds.), *Electrochem. Water Wastewater Treat.*, Butterworth-Heinemann,
953 2018: pp. 133–164. <https://doi.org/10.1016/B978-0-12-813160-2.00006-7>.

954 [108] L. Gui, H. Jin, Y. Zheng, R. Peng, Y. Luo, P. Yu, Electrochemical Degradation of
955 Bisphenol A Using Different Modified Anodes Based on Titanium in Aqueous Solution,
956 *Int. J. Electrochem. Sci.* 13 (2018) 7141–7156. <https://doi.org/10.20964/2018.07.76>.

957 [109] G.R. Salazar-Banda, G. de O.S. Santos, I.M. Duarte Gonzaga, A.R. Dória, K.I. Barrios
958 Eguiluz, Developments in electrode materials for wastewater treatment, *Curr. Opin.*
959 *Electrochem.* 26 (2021) 100663. <https://doi.org/10.1016/j.coelec.2020.100663>.

960 [110] W. Yang, N. Oturan, S. Raffy, M. Zhou, M.A. Oturan, Electrocatalytic generation of
961 homogeneous and heterogeneous hydroxyl radicals for cold mineralization of anti-cancer
962 drug Imatinib, *Chem. Eng. J.* 383 (2020) 123155.
963 <https://doi.org/10.1016/j.cej.2019.123155>.

964 [111] F.C. Moreira, R.A.R. Boaventura, E. Brillas, V.J.P. Vilar, Electrochemical advanced
965 oxidation processes: A review on their application to synthetic and real wastewaters,
966 *Appl. Catal. B Environ.* 202 (2017) 217–261.
967 <https://doi.org/10.1016/j.apcatb.2016.08.037>.

968
969

970 **Table 1.** Recent studies on decontamination of dye solutions by anodic oxidation method.

Pollutants	Conditions	Maximum degradation	References
Acid red18	-Ti/ Graphite felt/ Granular activated carbon (GAC) in fluidized bed. -Optimal conditions: $C_0 = 100 \text{ mg L}^{-1}$, 100 mM NaCl, pH = 3, $j = 20 \text{ mA cm}^{-2}$, GAC = 250 mg L^{-1}	96.5% of color removal and 84.8% of COD removal at 45 min	[3]
Acid blue 29	-Sn-Cu-Sb/SS -Optimal conditions: $C_0 = 60 \text{ mg L}^{-1}$, $j = 10 \text{ mA cm}^{-2}$, pH = 7, 50 mM Na_2SO_4	100% of COD removal at 600 min	[2]
Orange G	-BDD/SS -Conditions: 100 cm^3 of 0.52-6.34 mM of Orange G azo dye, pH 3, 50 mM Na_2SO_4 , and current density between 33.3 and 150 mA cm^{-2}	-100 %TOC removal in less than 330 min operating at $j \geq 66.7 \text{ mA cm}^{-2}$ -100% Color removal at 396 min-at 150 mA cm^{-2} .	[36]
indigo carmine	-BDD/SS -Conditions: indigo carmine up to 0.9 g L^{-1} , 50 mM Na_2SO_4 , pH 3.0-10.0, and 100, 300, and 450 mA at 35°C .	TOC reduced with current. 100% mineralization drops from 600 min at 100 mA to 300 min at 450 mA.	[37]

Methyl Violet	-BDD or Pt/SS	- BDD, >97% TOC decay	[38]
	-Conditions: 100 cm ³ of 100 mg L ⁻¹ , 50 mM Na ₂ SO ₄ , pH 3.0-7.4, current density 33.3- 150 mA cm ⁻²	with 18 Ah dm ⁻³ (360 min) at pH 3.0 and 15 Ah dm ⁻³ (300 min) at pH 7.4	
		- Pt TOC decay, close to 22% and 33% at pH 3.0 and 7.4.	
Reactive Black 5	-Ti/RuO ₂ /IrO ₂ /TiO ₂ /SS	-100 % of color removal and 33% of COD decay at 15 min.	[39]
	Optimal conditions: C ₀ =300 mg L ⁻¹ , 100 mA cm ⁻² , 8 mM NaCl		
Methyl orange	-Ti ₄ O ₇ / Ti	-Complete color removal and 91.7% COD reached after 5 h electrolysis	[40]
	-Conditions: C ₀ = 100 mg L ⁻¹ , 10 mA cm ⁻² , 100 mM NaCl		

971 **COD:** Chemical Oxygen Demand; **TOC :** Total Organic Carbon; **SS:** stainless steel

972

973

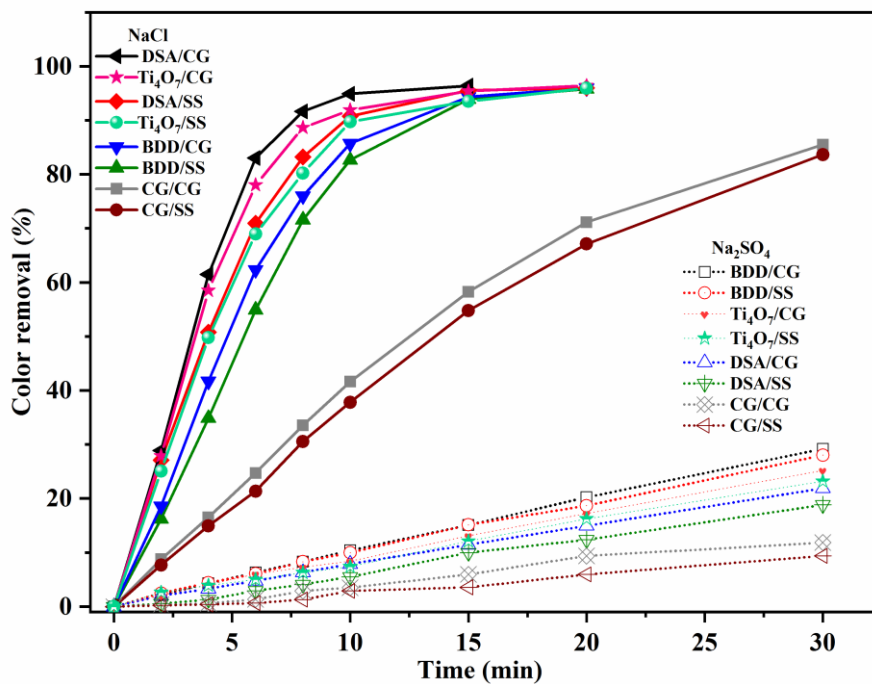


Figure 1: Kinetics of color removal (%) on different electrode materials; 40 mg L⁻¹ DR23, 25 mM NaCl or 12.5 mM Na₂SO₄, 8.3 mA cm⁻², pH = 6.0.

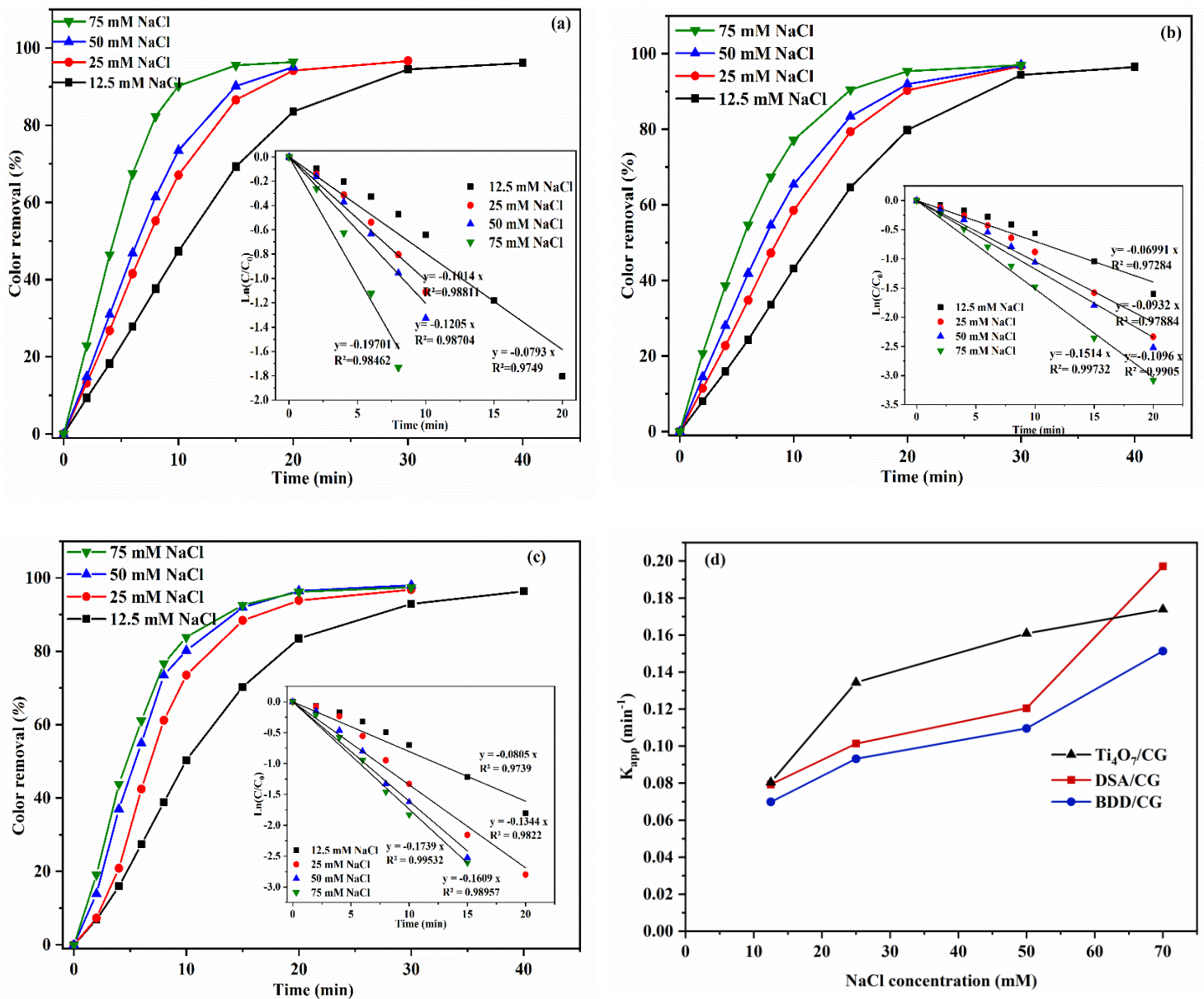


Figure 2: Effect of NaCl concentration, 60 mg L⁻¹ DR23, pH = 6.0, 5 mA cm⁻², (a) color removal (%), (a): DSA/CG, (b): BDD/CG, (c): Ti₄O₇/CG, and (d): the apparent kinetic rate constants vs. NaCl concentration. The insert panels are the kinetic analysis assuming a pseudo first order reaction.

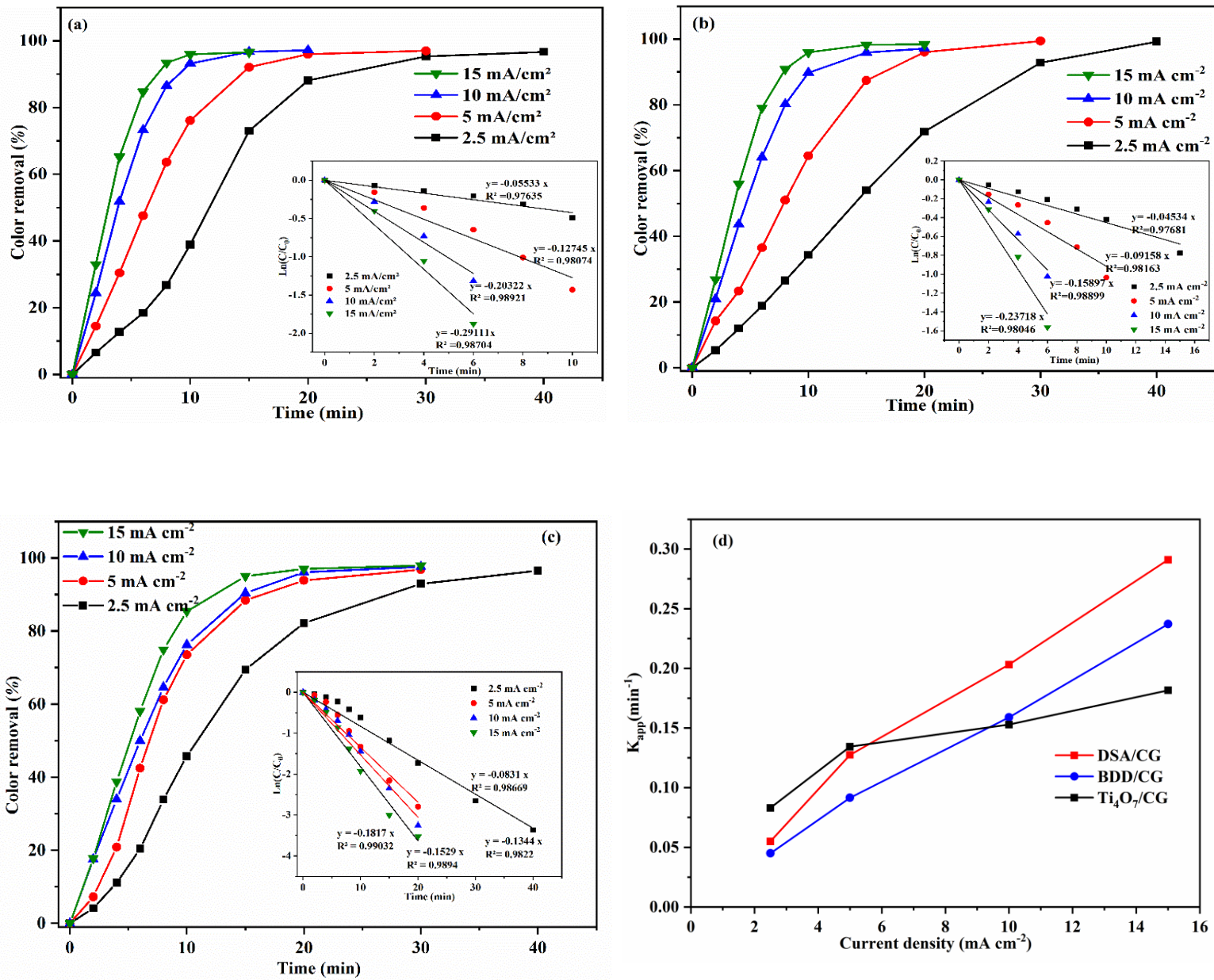


Figure 3: Effect of the current density, 60 mg L⁻¹ of DR23, 25 mM NaCl, pH = 5.89, (a): DSA/CG, (b): BDD/CG, (c): Ti₄O₇/CG, and (d): apparent kinetic rate. The insert panels are the kinetic analysis assuming a pseudo first-order reaction.

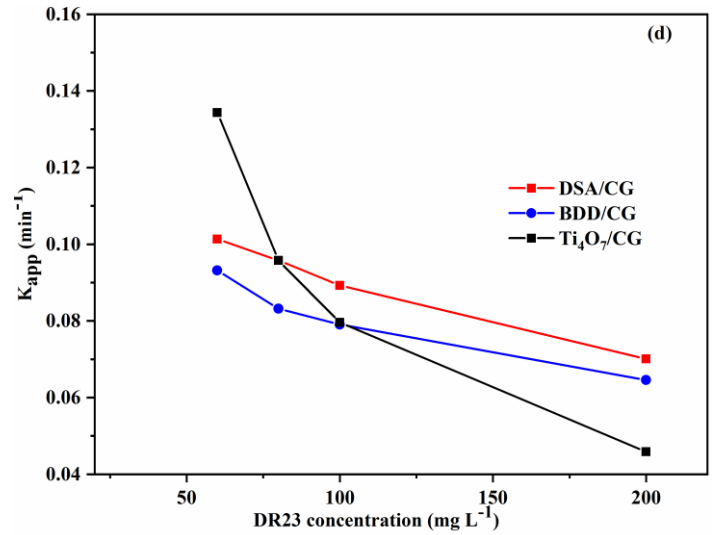
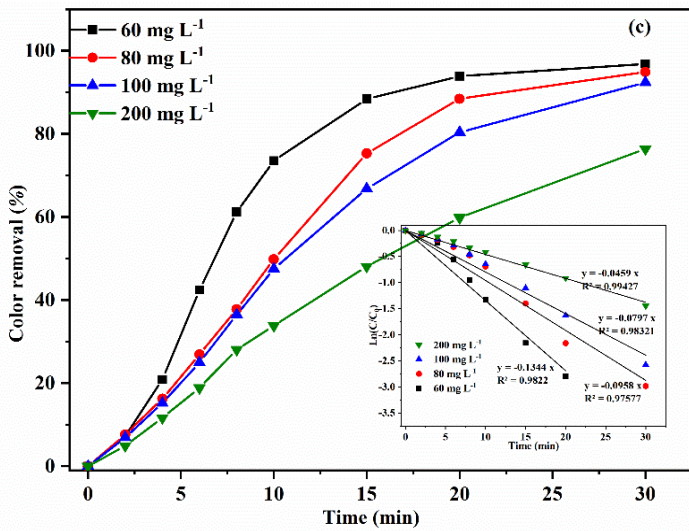
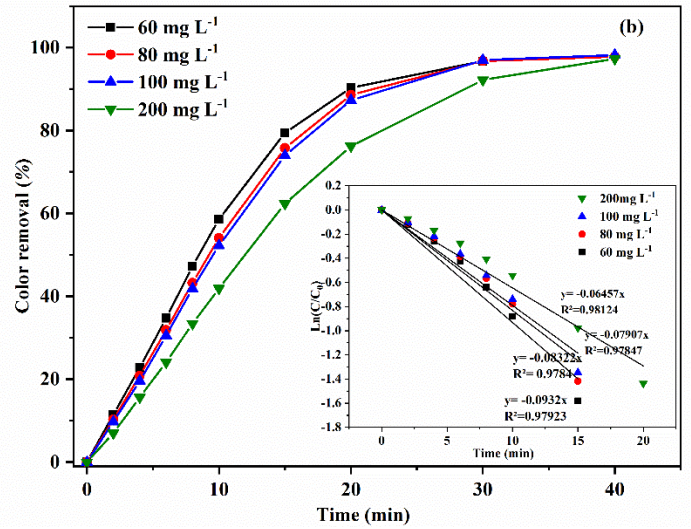
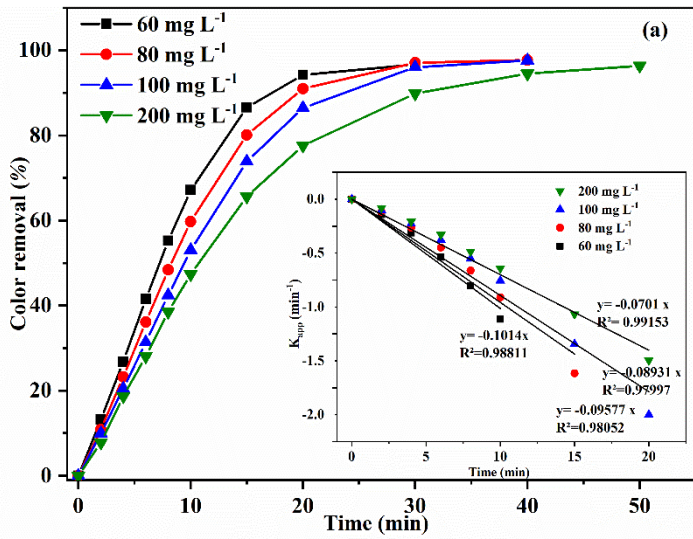


Figure 4: Effect of the initial dye concentration, 25 mM NaCl, pH = 5.89, 5 mA cm⁻² (a): DSA/CG, (b): BDD/CG, (c): Ti₄O₇/CG, and (d): variation of apparent kinetic rate. The insert panels are the kinetic analysis assuming a pseudo first order reaction.

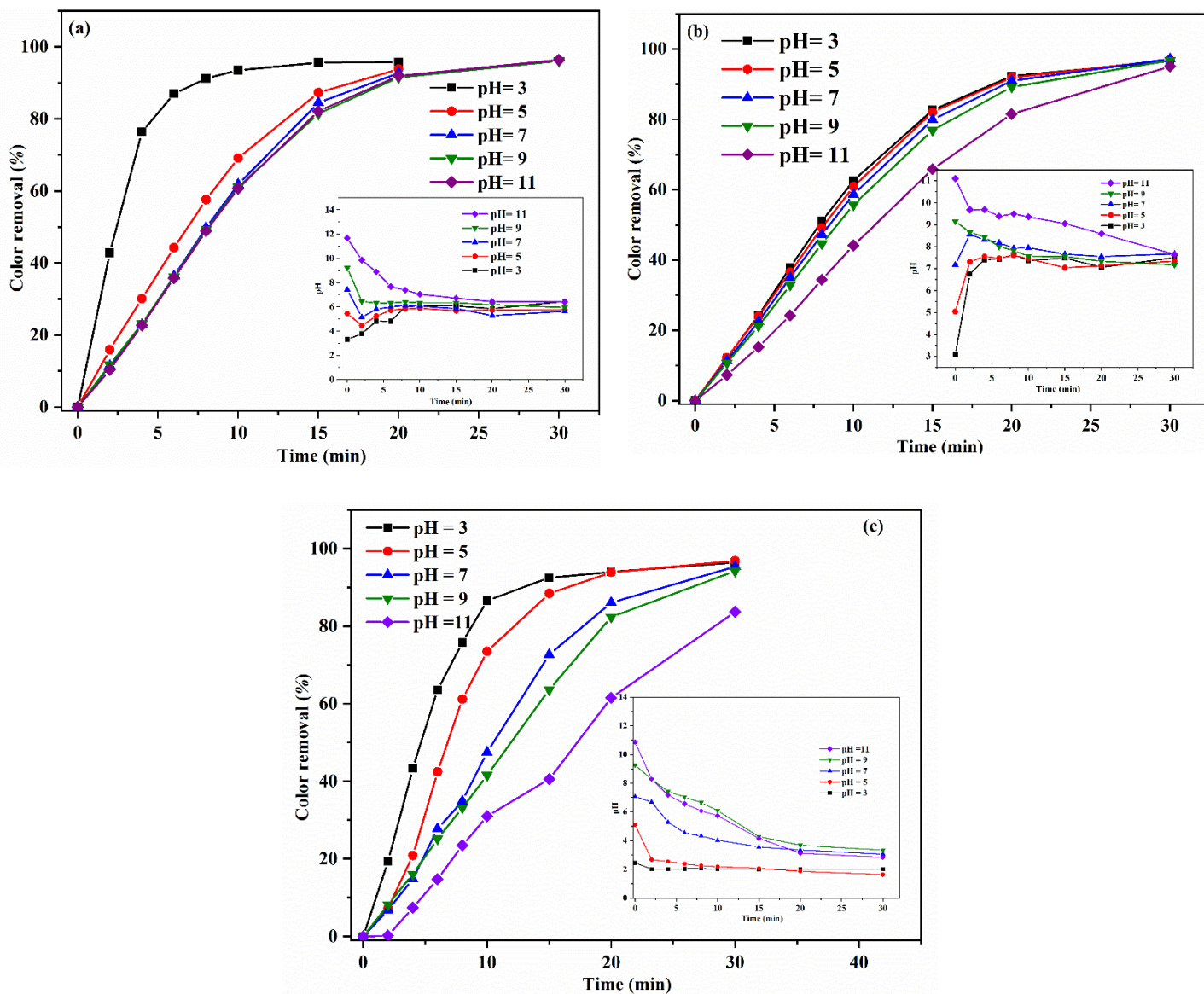


Figure 5: Effect of the initial pH on the color removal, 60 mg L⁻¹ of DR23, 25 mM NaCl, 5 mA cm⁻². Insert panels: variation of pH vs. time, (a): DSA/CG, (b): BDD/CG, and (c): Ti₄O₇/CG

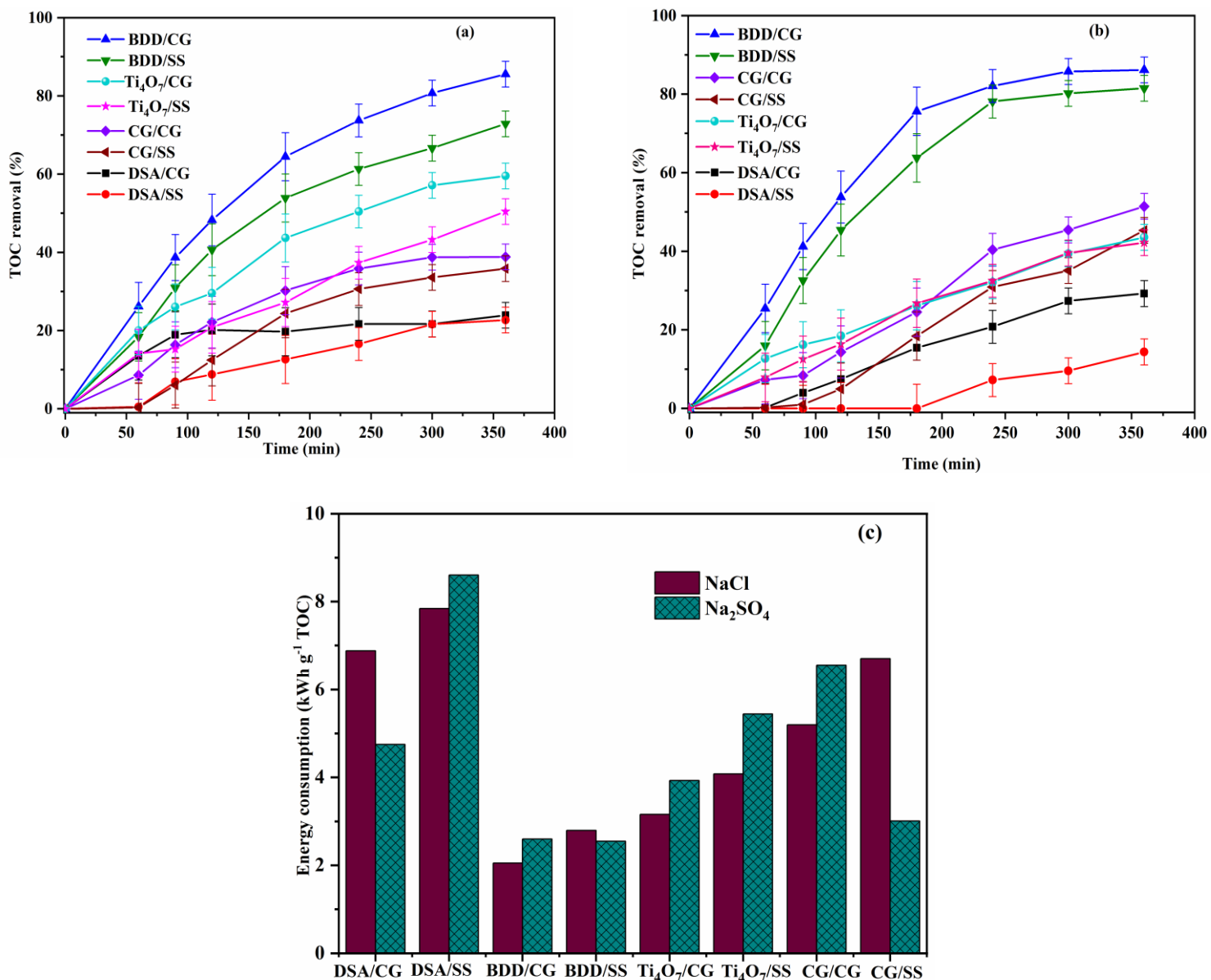


Figure 6: TOC removal vs. electrodes nature, 60 mg L⁻¹ of DR23, pH = 3.00, and 5 mA cm⁻², after 6h of electrolysis time, (a): 25 mM NaCl, (b): 12.5 mM Na₂SO₄, (c): Energy consumption for tested systems, kWh g⁻¹ TOC

TOC

980

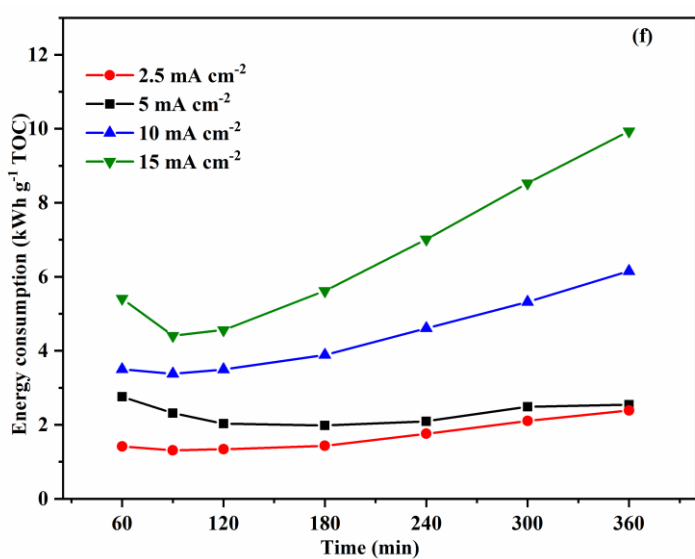
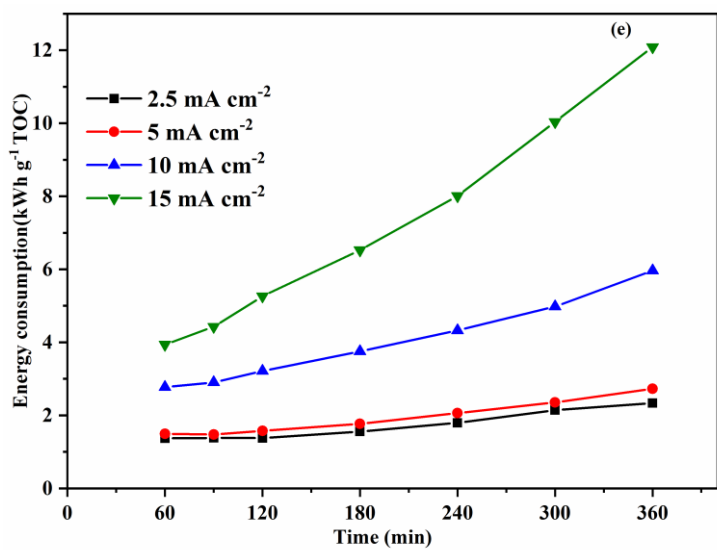
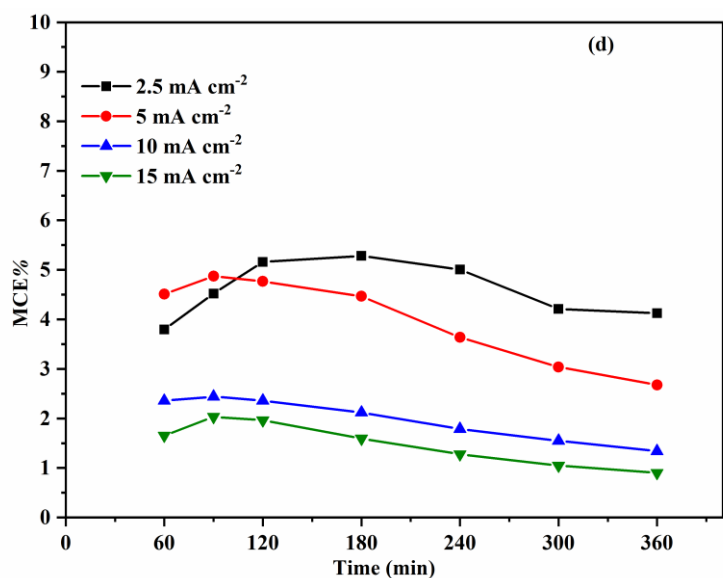
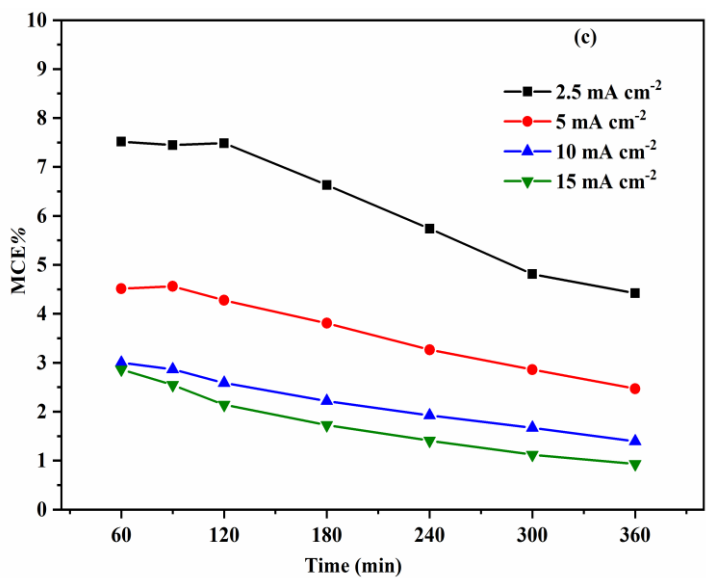
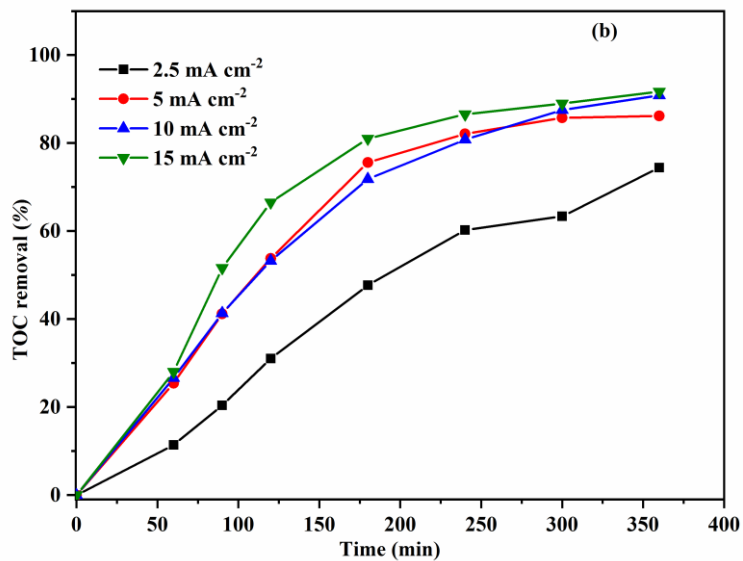
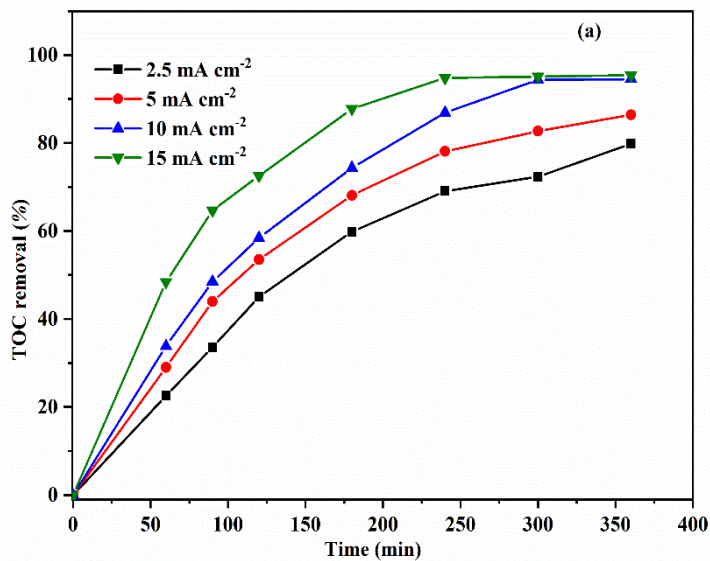


Figure 7: Effect of current on the mineralization of 60 mg L⁻¹ DR23 vs. time, (a, c, e) 25 mM NaCl, (b, d, f) 12.5 mM Na₂SO₄, pH = 3.00, BDD/CG, (a, b) TOC removal, (c, d) mineralization efficiencies (MCE%), (e, f) Energy consumption (kWh g⁻¹ TOC)

981